N° Ordre……../Faculty/UMBB/2024

People's Democratic Republic of Algeria
Ministry of Higher Education and Scientific Research

University of M'Hamed Bougara - Boumerdes
Faculty of Hydrocarbons and Chemistry
Department of Minerals and Petroleum Plays

Final Thesis
In order to obtain

MASTER's Degree

Field: Hydrocarbons

Option: Petroleum Geology

Presented by

AICHE Oussama

BELGHIT Abdeldjalil

Theme

Leveraging Artificial Intelligence to Re-evaluate Unconventional Hydrocarbon Potential: The Frasnian Source Rock in the North of Berkine Basin

In front of the jury:

Mrs CHAOUCHI Rabah	**Prof**	**UMBB**	**President**
Mrs SADAOUI Moussa	**Prof**	**UMBB**	**Examinator**
Mis YAHIAOUI Lamia	**MAA**	**UMBB**	**Examinator**
Mis BENAYAD Soumya	**MCA**	**UMBB**	**Supervisor**

Academic Year: 2023/2024

Acknowledgments:

First and foremost, I would like to praise Allah, the Most Gracious and the Most Merciful, the protector and constant companion in our lives. His infinite mercy has been the key to the success of this work.

***Ms. BENAYAD**, we would like to express our deep gratitude to you for your essential role as the supervisor of our thesis. and believed in us and adapted our ideas, Your commitment, expertise, and unwavering support have been crucial elements of our academic success, and we warmly thank you for your invaluable contribution.*

Your passion for research and dedication to your role as a supervisor have been a constant source of inspiration for us. Your insightful advice, availability, and ability to guide us throughout this process have been invaluable. Thanks to your support.

*We would also like to express our gratitude to **Ms. SERBAH Samira,** our co-supervisor, and **Mr. TABET Salim** and **Mr. MOKRI Yacine,** for their invaluable support throughout our thesis. Their contributions in terms of advice, expertise, and constructive feedback have greatly enriched our work. Their active involvement and interest in our research project have been key factors in our academic progress. We are sincerely grateful for your involvement and support.*

*And a special thanks to our professors **Mr. CHAOUCHI** and **Mr. SADAOUI** , and **Ms. KECIR** who pave who paved the way to knowledge and whose advice made us adore the field.*

Dedication

Dedicate this humble work to the greatest person in my life, **my mother**. Her unwavering love and support have been the cornerstone of my journey. She is the reason I am here, the one who has nurtured my dreams and lifted me up every time I stumbled. To **my father**, who has alwys cares about, teaching me the ways of life and standing by me through thick and thin.

To my little brother, **Raid Abdenacer,** whose enthusiasm and energy inspire me every day, and to my little sister **Rodain**, the princess of our family, whose smiles light up my world.

I also dedicate this work to my uncle, **Salaheddine Aiche**, whose dedication to this field has been a source of inspiration and whose constant encouragement has driven me to strive for excellence. To my lovely aunt **Rabiaa** and all my family, whose unwavering support has been my anchor.

I am deeply grateful to my thesis partner, **Abd Eldjalil**, the best person I've met at university. Your friendship and collaboration have not only made this work a success but have enriched my academic journey in countless ways.

To my dear friends, the future dentist **Haithem Sai** and **Hamoudi Diaa Eddine**, The future electrician **Faycel LAACHIBI ,**you have been and always will be special to me. Your camaraderie and support have been invaluable.

A special dedication goes to my middle school teacher, Mme. **MEWAFEK El Amria**, who believed in me and made me feel special, To my English teacher, **Kebaili**, **Yekhlef dounia** and my high school teachers, Ms. **Chebli** and **Brahimi Mouna**, your guidance and belief in me have shaped my path.

I also extend my heartfelt thanks to **Adel Maazouz** and his mother , **Hicham Boutaleb** for their steadfast support during this year.

To all the workers at SONATRACH Company, especially **Slimane**,**Abdelghani.**

Lastly, to all my classmates of **MAGL19**, especially **Souiki**, **Assad**, and **Aziz**

A special thanks to **Ms. Berour** and **Ms. Lamraoui** for their unwavering support.

AICHE Oussama

Dedication

I would like to express my heartfelt gratitude to a number of people whose support and encouragement have been instrumental in my journey.

First and foremost, I want to thank **my mother**, whose unwavering support and endless sacrifices have been a cornerstone in my life. Her guidance, love, and encouragement have helped shape the person I am today. Her nurturing spirit and dedication to our family have always been a source of inspiration.

I also extend my deepest gratitude to **my father**, who has been a constant pillar of strength and support. His presence and belief in me have given me the confidence to pursue my dreams and overcome any challenges that came my way.

To my sister, **Malak**, and my brother, **Ayoub**, your companionship and love have made my life richer and more meaningful. Thank you for always being there for me, through thick and thin.

I am incredibly grateful to **my grandmothers**, whose love and prayers have always been a protective shield around me. **Ma Meriem** and **Zahia**, whose prayers have been a constant source of comfort and strength. To **my grandfather** and all **my aunts** and **uncles** and **cousins,** thank you for your unwavering support and love. In particular, I would like to thank my aunt **Samia** and her children, **Mimi**, **Ayah**, and **Boualem**. Your warmth and hospitality made me feel at home even when I was far away, and your kindness will always be remembered.

To my friends, **Kader**, **Abdallah**, **Yanis** ,**Oussama Rahmani** and to my my thesis partner **Oussama** and all the friends I have met throughout my life, your companionship and support have been invaluable. Each one of you has contributed to my journey in a unique and meaningful way.

I also extend my thanks to my friends from **MAGL19**, especially **Asaad** and **Aziz**.

A special thanks to **Ms. Berour** and **Ms. Lamraoui** for their unwavering support and guidance.

BELGHIT Abdeldjalil

Abstract

In this study, we focused on the geochemical evolution of shale gas within the Frasnian source rock, situated in the Berkine Basin of the Algerian Sahara. Our primary objective was to analyze the geochemical properties of the Frasnian formation to estimate the volumes of hydrocarbons present, employing the methodology proposed by Michael (2014).

Our results reveal that the Frasnian formation is rich in organic matter and possesses substantial petroleum potential. However, it is crucial to note that the exploitation of these resources necessitates the use of advanced technologies, given that the Frasnian formation is classified as an unconventional resource. Furthermore, we incorporated artificial intelligence techniques to refine the estimation of hydrocarbon volumes, thereby enhancing the accuracy of our assessments

Résumé

Dans ce travail, nous nous sommes concentrés sur l'évolution géochimique du gaz de schiste dans la roche mère du Frasnien, située dans le bassin de Berkine, dans le Sahara algérien. Notre objectif principal était d'analyser les propriétés géochimiques de la formation Frasnien afin d'estimer les volumes d'hydrocarbures présents, en utilisant la méthode Michael (2014).

Nos résultats indiquent que cette formation contient des quantités significatives de matière organique et présente un potentiel pétrolier considérable. Cependant, il est important de souligner que le développement de ces ressources nécessite des technologies spécialisées, car la formation Frasnien est considérée comme une ressource non conventionnelle. De plus, nous avons intégré des techniques d'intelligence artificielle pour améliorer l'estimation des volumes d'hydrocarbures

ملخص

في هذا العمل، ركزنا على التطور الجيوكيميائي للغاز الصخري في صخرة المصدر الفرسني، الواقعة في حوض بركين في الصحراء الجزائرية. كان هدفنا الرئيسي هو تحليل الخصائص الجيوكيميائية لتقدير أحجام المحروقات الموجودة في فراسنيان باستخدام طريقة مايكل 2014.

تشير النتائج التي توصلنا إليها إلى أن هذا التكوين يحتوي على كميات كبيرة من المواد العضوية وله إمكانات نفطية كبيرة. ومع ذلك، من المهم التأكيد على أن تطوير هذه الموارد يتطلب تكنولوجيات متخصصة، حيث أن تكوين فراسنيان يعتبر موردا غير تقليدي. بالإضافة إلى ذلك، قمنا بدمج تقنيات الذكاء الاصطناعي لتعزيز تقدير أحجام الهيدروكربونات المحروقات

Table of contents :

Figures caption:

Figure 1: Map of Algeria showing the distribution of shale gas and shale oil resources over the Saharan platform.

Figure 2: A: Map of Algeria showing the location of Berkin Basin.

B: Location map showing Northern Timissit.

Figure 3: Lithostratigraphic Log of the Berkine Basin.

Figure 4: The major structural evolutions of the Berkine Basin.

Figure 5: Organic matter observation in well Z-1 at Depth 3658.34m.

Figure 6: Mineralogical variation profile as a function of well depth.

Figure 7: Ternary diagram illustrating minerals observed within the Frasnian source rock.

Figure 8: Rock-Eval 6 Turbo results.

Figure 9: Example of organic matter observation.

Figure 10: Total Organic Carbon (TOC) variation profile as a function of depth in well Z-1.

Figure 11: Free potential (S1) variation profile as a function of depth in well Z-1.

Figure 12: Profile of variation of residual potential (S2) as a function of depth in well Z-1.

Figure 13: Classification of the quantity of S2 in well Z-1.

Figure 14: Maturation diagram according to Interpreted Pyrolysis (IP) and Tmax of well Z-1.

Figure 15: Diagram of Hydrogen Index (HI) as a function of Oxygen Index (OI) and diagram of Tmax / HI showing different types of kerogens in the Frasnian source rock.

Figure 16: Microscope photo of the organofacies of sample 3668.40m.

Figure 17: Maturity scales and hydrocarbon products.

Figure 18: Variation profile of adsorbed fraction as a function of well depth in Z-1.

Tables caption:

Table 1: Evolution of Shale Gas Production in Algeria.

Table 2: Coordinates of the Northern Timissit perimeter.

Table 3: Summary of samples used in mineralogical and petrographical analysis.

Table 4: Mineralogical results by X-rays of well Z-1/2019.

Table 5: Classification of rocks by organic carbon richness.

Table 6: Classification of the amount of TOC in well Z-1.

Table 7: Classification of the amount of S1 in well Z-1.

Table 8: Summary of the results of the micros and their maturity.

Table 9: Calculation of the numerical application of the adsorbed fraction.

Table 10: Computations of the numerical application of the evaporitic loss and the S1 well correction Z-1.

Table 11: Calculations of the OSI (oil saturation index) well Z-1 index.

Table 12: Computations of the numerical application of the mass to volume conversion of hydrocarbons from wells Z-1.

Symbols:

APL: Analyzed Polarized Light

DXR: Diffraction X-Ray

TOC: Total Organic Carbon (%)

S1: Quantity of free hydrocarbons in the rock (mg HC/g rock)

S2: Quantity of hydrocarbons released by kerogen during pyrolysis (mg HC/g rock)

S3: CO2 released by kerogen during pyrolysis (mg CO2/g rock)

IH: Hydrogen Index (mg HC/g TOC)

IO: Oxygen Index (mg CO2/g TOC)

OSI: Oil Saturation Index (mg HC/g TOC)

PP: Petroleum Potential (mg HC/g rock)

IP: Production Index (ranging from 0 to 1)

Tmax: Temperature at peak generation during pyrolysis (°C)

TAI: Thermal Alteration Index (1 – 4) Chevron

α : The coefficient of the HC Loss correction

dr : The density of the source rock

dhc: The density of hydrocarbons

VOL : The volume in place

AI : Artifical intelligence

General Introduction

The growing demand for hydrocarbons and natural gas in the international market is driven by various factors, including increased energy consumption. However, existing conventional resources, such as easily accessible oil and natural gas, are limited and cannot meet this rising demand. As a result, many countries are turning to the development of their unconventional resources to bridge the gap between supply and demand. These unconventional resources include shale gas, oil sands, coalbed methane, and other forms of hydrocarbons that require advanced extraction methods.

In Algeria, the economic prospects offered by the Frasnian and Silurian shale formations, which are classified as world-class source rocks, are particularly promising. For several years, Algeria, through its national oil company Sonatrach, has been conducting studies to evaluate the potential of shale gas. The Berkine Basin has emerged as one of the richest hydrocarbon basins in the country.

The Frasnian source rock, a sedimentary rock, exhibits unique geochemical characteristics and a geological history that suggest it has a high potential for containing large volumes of shale gas. Consequently, we have chosen the Frasnian source rock to estimate the potential of shale gas.

Artificial Intelligence (AI) plays a crucial role in the analysis and evaluation of unconventional resources. By utilizing advanced data processing techniques, geological modeling, and predictive analyses, AI can enhance the accuracy of reserve estimates and optimize exploration and production processes.

This work is structured into six chapters:

1. **Chapter 1**: Provides a general overview of the potential for shale gas in Algeria.
2. **Chapter 2**: Offers an overview of the Berkine Basin and the Northern Timissit Perimeter, including a detailed presentation of the Berkine Basin and the study area.
3. **Chapter 3**: Discusses the methodology for the mineralogical and petrographical evaluation of the Frasnian source rock.
4. **Chapter 4**: Focuses on the geochemical evaluation of the Frasnian source rock, including geochemical analyses and their implications.
5. **Chapter 5**: Covers the estimation of hydrocarbon volumes in the Frasnian source rock using the Michael (2014) method.
6. **Chapter 6**: Integrates artificial intelligence into the estimation of hydrocarbon potential, applying AI techniques to enhance the estimation process.

CHAPTER 1 :”Overiew of Shale Gas in Algeria”

CHAPTER 1 :"Overiew of Shale Gas in Algeria"

1. Introduction into shale gas:

The growing global demand for hydrocarbons and natural gas is primarily driven by increased energy consumption across various sectors. Conventional resources, such as easily accessible oil and natural gas, are increasingly unable to meet this surging demand. Consequently, many countries are now focusing on the development of their unconventional resources to bridge the gap between supply and demand. Unconventional resources include shale gas, oil sands, coalbed methane, and other forms of hydrocarbons that necessitate advanced extraction technologies and methodologies.

2. History of the production of Shale Gas in Algeria:

Interest in shale gas in Algeria began in the early 2010s as the government sought to diversify its energy revenue and increase proven gas reserves. Geological and seismic studies identified significant potential in the Sahara's Ahnet and Berkine basins. The first exploratory drilling took place in 2014, led by the national hydrocarbons company, Sonatrach, in collaboration with experienced foreign firms.

According to the International Energy Agency, Algeria holds an estimated 20,000 billion cubic meters of technically recoverable shale gas. However, the development of this resource has faced significant hurdles. In 2015, local opposition and environmental concerns, particularly in the region of In Salah, brought attention to risks such as groundwater contamination and induced seismic activity. These concerns highlighted the environmental and social challenges associated with shale gas exploitation.

Economic and technical challenges also impact the viability of large-scale shale gas production. Fluctuating oil and gas prices have further complicated investment and planning. Despite these obstacles, the Algerian government remains committed to integrating shale gas into its energy strategy. Efforts are ongoing to improve regulatory frameworks, attract foreign investment, and develop safer, more efficient extraction technologies.

Sonatrach continues to play a central role in these endeavors, investing heavily in research and development to advance exploration and production techniques. The company is focused on overcoming the technical and environmental challenges to unlock the full potential of Algeria's substantial shale gas reserves, ensuring they contribute to the country's energy security and economic growth.

Year	2014	2015	2016	2017	2018	2019	2020	2021	2022	2023
Production of shale gas (milliards of m^3)	6	8.2	7	7.8	9	9.8	10	22,8	30	20

Table 1: The evolution of the production of Shale Gas in Algeria (APS, 2024)

3.Distribution of prospection of Shale Gas Reserves in Algeria :

Algeria's shale gas reserves are primarily concentrated in several key basins. The Ahnet Basin holds the largest share, containing 35% of the reserves, followed by the Berkine Basin with 30%. The Timimoun Basin and the Reggane Basin account for 15% and 10% of the reserves, respectively, while the remaining 10% is distributed among other basins.

The national hydrocarbon company, Sonatrach, has initiated a pilot project in the Ahnet Basin, located in the south of the country. This project aims to commence commercial production of shale gas by 2022. As part of this initiative, eleven shale gas exploration wells are scheduled to be drilled between 2021 and 2027.

CHAPTER 1 :"Overiew of Shale Gas in Algeria"

Algeria boasts two major shale formations: the Silurian Tannezruft shale and the Devonian Frasnian shale. The country encompasses seven significant basins: Tindouf, Timimoun, Reggane, Ghadames/Berkine, Illizi, Mouydir, and the Ahnet Basin, as depicted in Figure 1. These basins collectively contain approximately 3,419 trillion cubic feet (tcf) of gas in place. Of this total, the technically recoverable quantity is estimated at 707 tcf, representing 20% of the total volume in place.

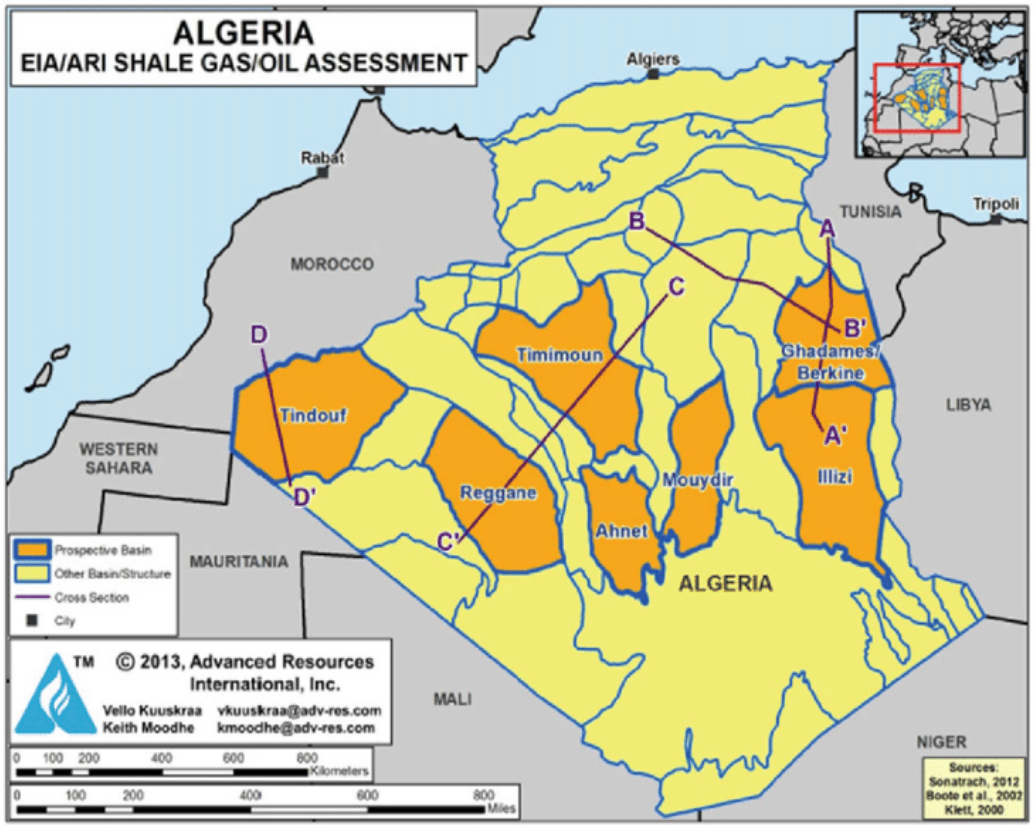

Source: ARI, 2013.

Figure 1: Map of Algeria showing the distribution of shale gas and shale oil resources over the Saharan platform (after EIA/ARI 2013)

CHAPTER 2 : “ Overview on the Berkin Basin and the Northen Timissit Perimeter”

1. Generalities on the Berkine basin :

1.1. Geographical and geological settings

The Berkine Basin is situated in the eastern part of the Saharan platform (Fig. 2), between latitudes 29°11' and 33°00' North, and longitudes 05°55' and 09°30' East. It covers an area of approximately 100,000 square kilometers.

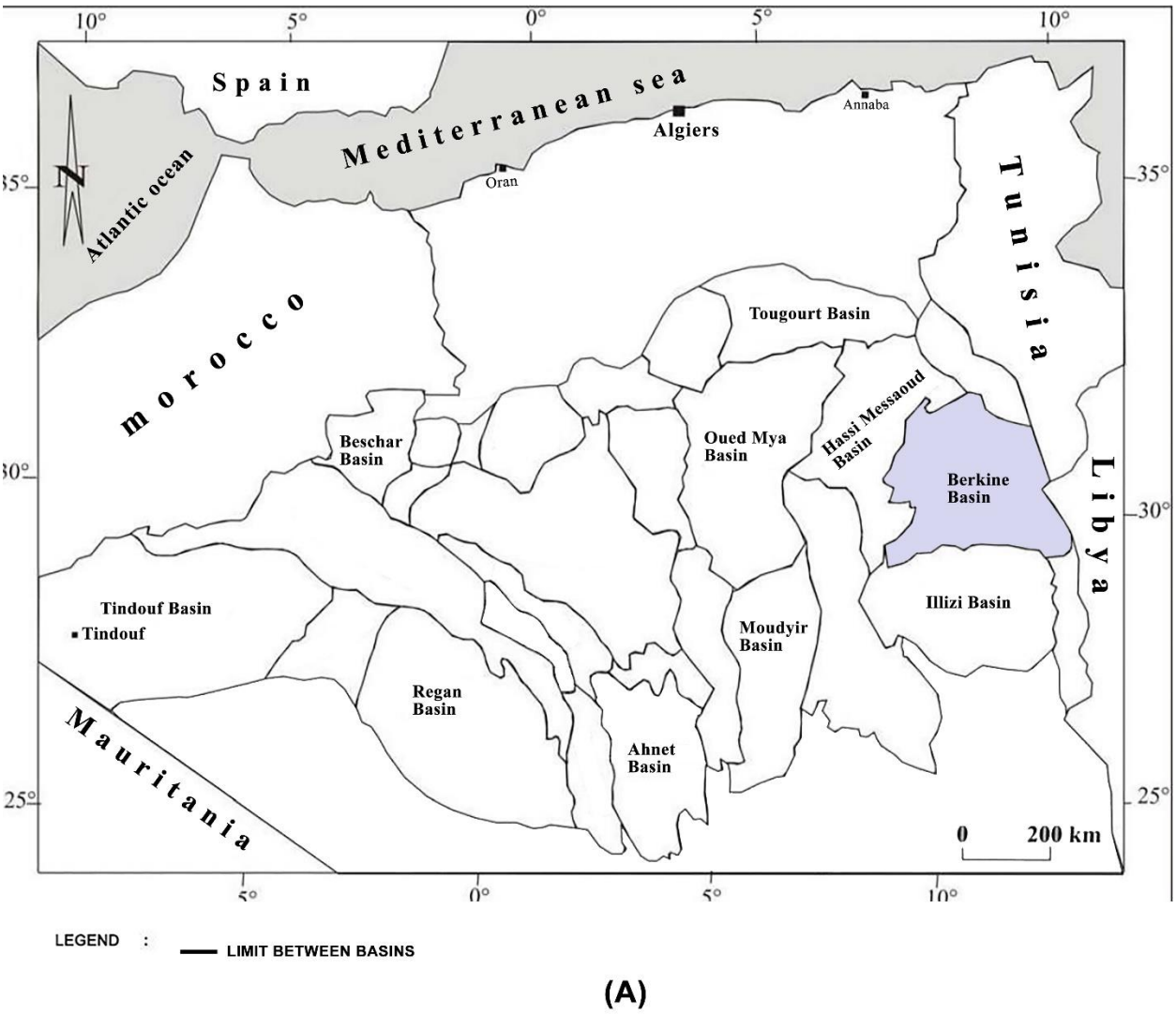

Figure 2 : Map of Algeria showing the location of Berkine Basin (WEC 2007)

2. Stratigraphical settings

The Berkine Basin retains a sedimentary fill of over 6000 meters in thickness, particularly at the basin's center, ranging from the Paleozoic to the present day. These sedimentary rocks overlay a Precambrian granitic basement. Magmatic rocks, the focus of this study, are also abundant subsurface within the sedimentary series.

The Paleozoic (from Cambrian to Lower Carboniferous) consists mainly of siliciclastic formations. The Mesozoic contains over 4 km of sediments, while Cenozoic formations are preserved mainly in the central part of the depression, reduced to a layer of less than 200 meters in thickness composed of Miocene and Pliocene sediments (Fig. 3).

2.1. The Paleozoic Era

2.1.1. Cambrian:

The Cambrian stage in the Berkine Basin, as classified by Aliev et al. (1971) and Fabre (1976), is characterized by sandstones and quartzites with conglomerate beds. These deposits are subdivided into three lithozones: R3, R2, and Ra, with an average thickness of 300 meters.

2.1.2. Ordovician:

Comprising marine deposits, the Ordovician system in the Berkine Basin consists of El Gassi clays, El Atchane sandstones, and Ouargla sandstones. Notably, these formations exhibit a glacial origin, with micro-conglomeratic clays and Ramade sandstones being prominent lithologies within the Ordovician succession.

2.1.3. Silurian :

The Silurian strata are primarily characterized by fossiliferous black clays overlain by clayey sandstones. These black clays are widely recognized as significant stratigraphic markers across the Saharan platform and serve as excellent source rocks. Two distinguished members within the Silurian succession are the Clayey Silurian or Graptolite Shales and Clayey-Sandy Silurian.

2.1.4. Devonian

In the Berkine Basin, the Devonian sequence is well-developed and subdivided into eight members or sub-stages, reflecting a diverse geological history and sedimentary evolution during this period

2.1.5. Carboniferous

The Carboniferous series, ranging in thickness from 1100 meters to 1500 meters, spans between the Tournaisien and Stéphanien stages. It primarily comprises black clay with individualized sandstone bodies, interspersed with numerous limestone banks.

2.2. Mesozoic Era

2.2.1. Triassic

Overlying the Paleozoic with a Hercynian unconformity, the Triassic formations mainly consist of evaporitic and clayey-sandy deposits, renowned for their reservoir potential. Subdivisions include the Lower Clayey-Sandy Trias (TAGI), Clayey-Carbonate Trias (TAC), and Upper Clayey-Sandy Trias (TAGS).

2.2.2. Jurassic

The Jurassic strata primarily comprise lagoonal marine sediments, commencing with a characteristic dolomitic level known as the "B horizon," which is ubiquitous across the basin.

2.2.3. Cretaceous

Consisting of alternating sandstones, clays, dolomites, and limestones, the Cretaceous formations also include beds of anhydrites, gypsum, and salts. Towards the upper sections, carbonate lithology become predominant.

2.3. Cenozoic Era

Mainly comprising detrital deposits from the Mio-Pliocene, the Cenozoic formations consist of translucent, yellowish sands with intermittent red-brown sandy clay layers and clayey limestone beds, reflecting relatively recent geological processes within the basin.

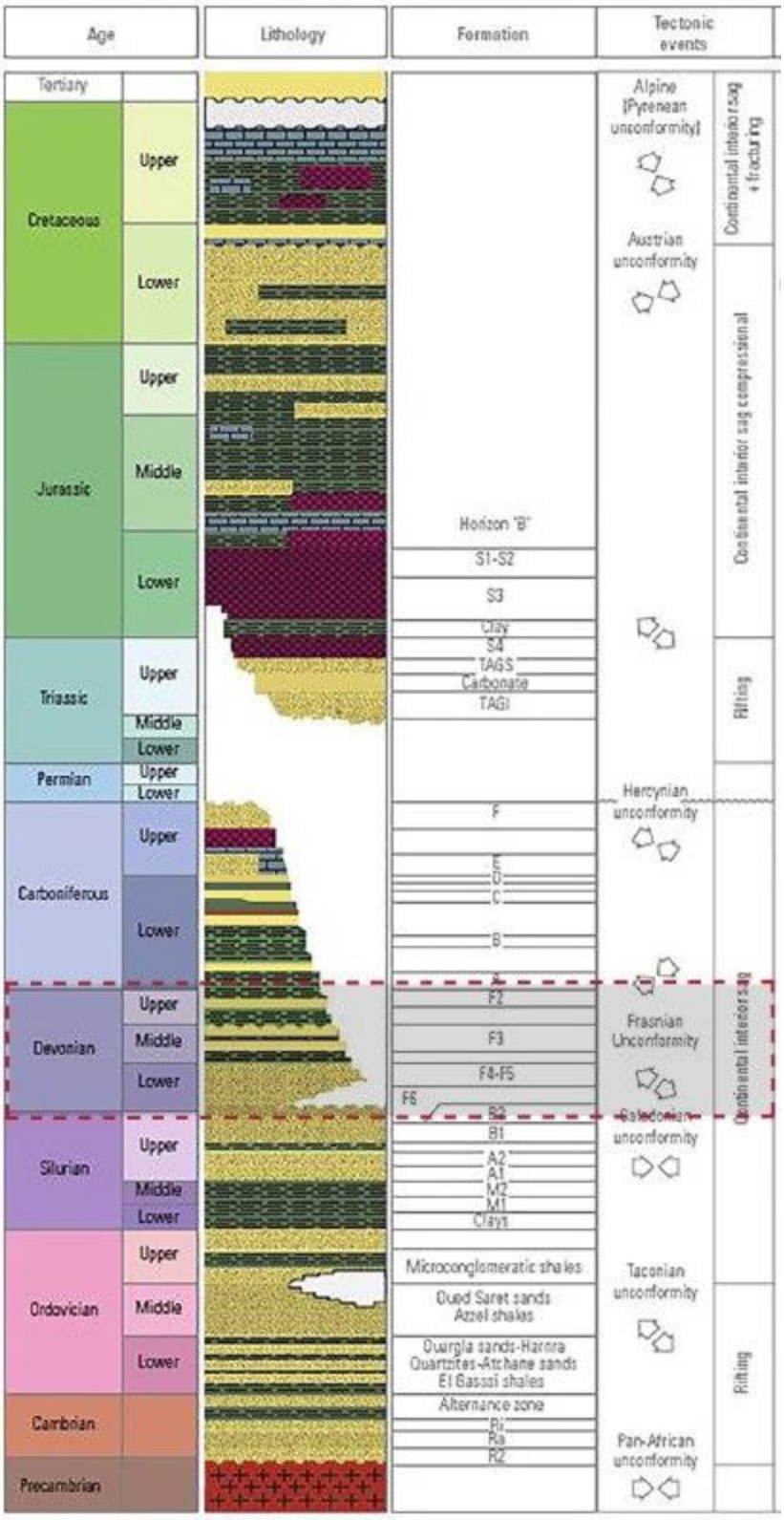

Figure 3: Lithostratigraphic Log of the Berkine Basin (Schlumberger 2007)

3. Structural and tectonic settings:

The structural and tectonic evolution of the Berkine Basin has been shaped by various phases since the Paleozoic era, contributing to its present-day geological framework.

3.1. Pan-African Phase :

During the Precambrian era, the Pan-African phase was marked by vertical sub-meridian faults resulting from collisional tectonics, laying the foundation for subsequent structural developments.

3.2. Cambrian Ordovician :

Following the Pan-African phase, a period of significant erosion occurred during the Cambrian-Ordovician era, leveling structures and reliefs. Distension along N-S faults led to variations in thickness and facies, indicating tectonic instability during sediment deposition.

3.3. Taconic Compression :

Subsequent to the Cambrian-Ordovician distension, the Taconic compression phase exerted pressure along the N-S faults, contributing to the basin's current architectural configuration.

3.4. Silurian Distension :

The Silurian era witnessed a distension phase following the melting of an ice cap, resulting in the deposition of black clays indicative of this period's tectonic activity.

3.5. Caledonian Compression:

A phase of general uplift and detrital deposition occurred between the Silurian and Devonian periods, known as the Caledonian compression, further shaping the basin's geological characteristics.

3.6. Devonian Phase:

is characterized by distinct events:

•Lower Devonian: Pre-existing thickness and facies variations indicate a distensive phase along sub-meridian structural axes.

• Middle and Upper Devonian: An erosional period, known as the Frasnian unconformity, marked by significant geological changes.(Fig.4.).

3.7. Hercynian Unconformity:

The Hercynian unconformity phase, affecting primarily the northern Berkine Basin, led to the cessation of Carboniferous sedimentation and the emergence of lagoonal deposits. Movements during this phase played a crucial role in structuring the Saharan platform basins.

3.8. Autrichian Phase:

Characterized by E-W compression, the Autrichian phase caused structural inversion, leading to the reversal of normal faults created during the Triassic and Jurassic sequences (Fig.4.).

3.9. Pyrenean Phase:

Finally, the Pyrenean phase, with its NW-SE directional compression, resulted in the formation of numerous anticlines, contributing further to the basin's structural complexity.

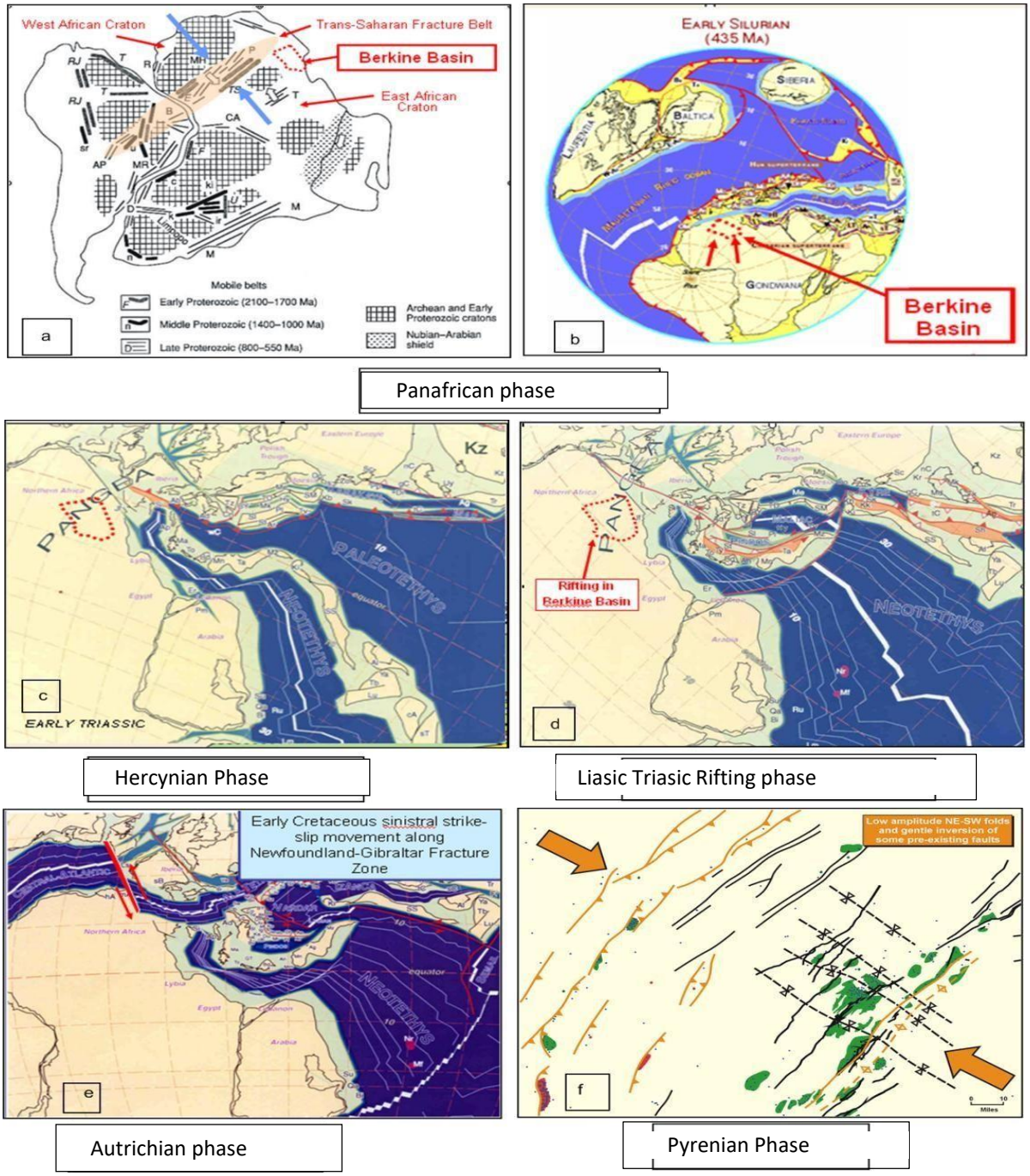

Figure 4: The major structural evolutions of the Berkine Basin (McKenna and Hedley, 2002)

4. Generalities about the Northern TIMISSIT Perimeter :

4.1. Geographical settings:

Situated in the southeastern region of the Berkine Basin, also referred to as the East Algerian Syncline between 4 summits (table.2.), the northern Timissit exploration perimeter (block 210) encompasses an area of approximately 2732.35 km2. This area is delineated by four distinct summits, contributing to its unique geological characteristics. With a substantial sedimentary coverage exceeding 6500 meters, the northern Timissit exploration perimeter offers considerable potential for geological exploration and resource assessment.

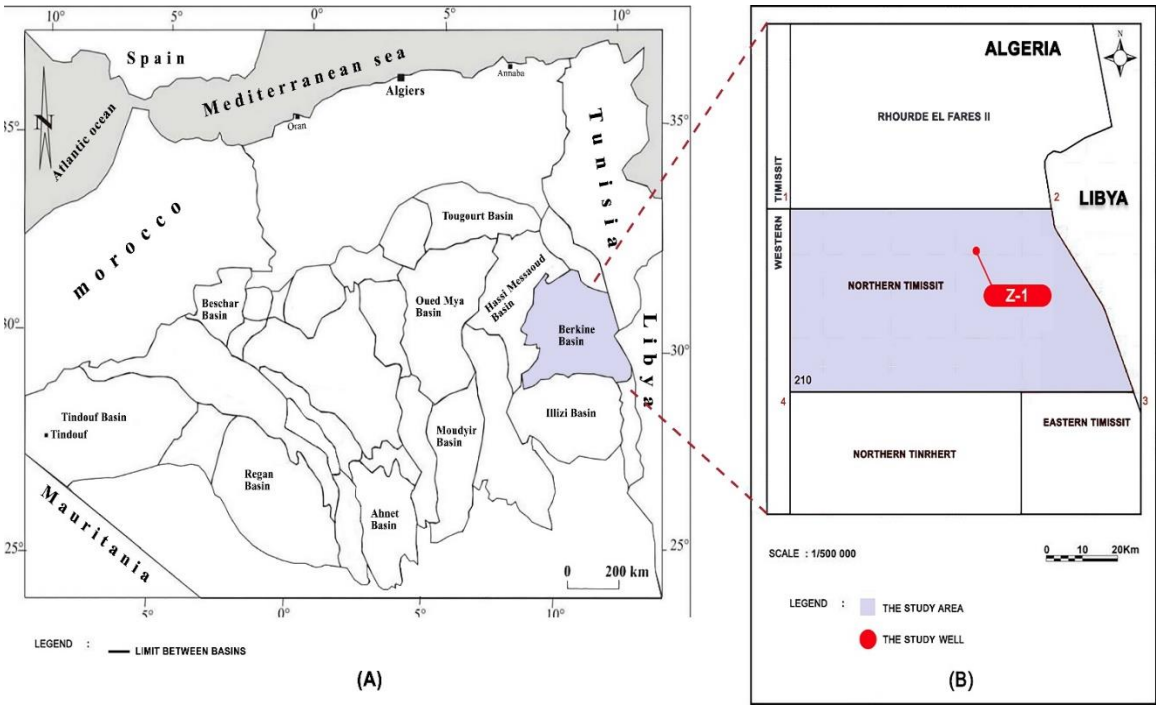

Figure:A: Map of Algeria showing the geographical location of the Berkine basin (WEC 2007).

B: location map showing Northern Timissit (SONATRACH 2019).

Summit	Longitude	Latitude
1	08°45’00’’E	30°05’00’’N
2	Algerian-Libyan borders	30°05’00’’N
3	Algerian-Libyan borders	29°45’00’’N
4	08°45’00’’E	29°45’00’’N

Table 2 : Coordinates of the The Northern Timissit perimeter (SONATRACH,2019)

4.2. Stratigraphical settings

Within Block 210, the stratigraphic succession mirrors that of the broader Berkine Basin (see Fig. 3). Paleozoic sequences dominate, characterized by clastic deposits spanning from the Cambrian to the Visean (Carboniferous). However, the Hercynian tectonic phase has eroded upper Carboniferous formations within this region. Mesozoic-Cenozoic sequences unconformably overlie the Paleozoic, featuring thick evaporitic series like the Lias, which form an effective regional cover for Triassic reservoirs.

4.3. Tectonic and structural settings:

The Timissit region has undergone several tectonic events, shaping its current structural settings (see Fig. 3):

4.3.1. Hercynian Compressive Cycle (Devonian-Carboniferous): Characterized by NE/SW and NW/SE compressive stresses, this phase led to the creation of NE/SW structures and progressive erosion of Paleozoic formations from southeast to northwest.

4.3.2. Post-Hercynian Extensional Phase (Upper Triassic/Lower Jurassic): Initially with NW/SE-oriented stresses, transitioning to NE/SW during the Jurassic, this phase created and reactivated NE/SW and NW/SE trending normal faults. It also caused lateral variations in facies and thicknesses of Triassic deposits due to syn-sedimentary tectonics, shaping narrow horsts and graben structures.y

4.3.3. Austrian Compressive Phase (Lower Cretaceous): Characterized by E/W

compressive stress, this phase transpressively impacted major NE/SW structural axes, resulting in numerous discoveries of deposits along these axes throughout the basin.

4.3.4. Tertiary Movements: Exhibiting relatively weak impacts compared to previous phases, Tertiary movements had limited effects in this region of the basin.

4.4. Source rocks

Principal source rock units within various formations capable of producing hydrocarbons in the Study Area include:

4.4.1. Lower Silurian: Comprising grey to black clays, often radioactive at the base, with thicknesses ranging from 10 m to 100 m. Total organic carbon (TOC) varies from 1% to 11%, reaching up to 20% in some instances. Organic matter of marine origin contributes to excellent quality source rock, with hydrocarbon potential often exceeding 60 kg hydrocarbon/t.

4.4.2. Lower Frasnian: Resulting from a relatively calm period marked by a marine transgression over most of the Saharan Platform, this formation exhibits thicknesses varying from 10 m to 240 m. TOC in the Lower Frasnian formation reaches up to 10%, with a potential of 52 kg hydrocarbon/ton. This formation is expected to contain condensate and gas and oil, presenting significant hydrocarbon potential.

CHAPTER 3 : Mineralogical and Petrograohical evaluation of the Frasnian source rock

1. Mineralogical and Petrophysical analysis of the Frasnian Source rock:

1.1.Methodology:

A total of twenty-two (22) thin sections (refer to Table 3) retrieved from Well Z-1 were meticulously examined using both natural light and polarized light transmission microscopy. This comprehensive approach enabled the identification of detrital and authigenic minerals, as well as the analysis of diagenetic phenomena, their evolution over time, and their chronological sequence.

Well	Core Number	Depth(m)	Number of Samples	
			Petrography (TS)	Mineralogy (TS)
Z-1	1	3583.86m- 3589.91m	3	3
	3	3595.34m- 3610.75m	5	5
	5	3615.76m- 3631.21m	5	5
	7	3639.45m- 3649.65m	4	4
	8	3654.67m	1	1
	9	3658.34m	1	1
	10	3663.8m- 3667.79m	2	2
	11	3671.15m	1	1
Total of samples			22	22

Table 3: Summary of samples used in mineralogical and petrographical analysis

1.2. Results

1.2.1. Diagenetic Processes

Throughout the geological history of Frasnian sediments, various physico-chemical changes occurred, leading to diagenetic phenomena that significantly influence the reservoir properties of the rock. By analyzing twenty-two (22) core samples from Well Z-1, the primary diagenetic processes identified that contribute to either the enhancement or degradation of reservoir qualities are:

1.2.1.1. Carbonate Cementing

Carbonates, primarily composed of calcite and dolomite, play a crucial role in Frasnian deposits. They are often formed in shallow marine environments through the dissolution/precipitation of mollusc shells. Calcite is observed either as quartz-sized grains scattered in the clay matrix or as irregular crystals of microsparity and sparite clogging the walls and structures of some bivalves. Meanwhile, dolomite is presented in small diamond crystals bathing in the clay matrix (refer to Board I, Picture D).

1.2.1.2. Silicification

Silicification, albeit observed in a minimal percentage in cores 01, 03, and 05, results in microgranular authigenic silica of millimetric size. This silica fills cavities or small irregular pockets of different sizes, either isolated in the clay matrix or forming aligned trails. The origin of this silica is likely from the dissolution of silica fossil tests during the early stages of sediment burial (refer to Board II, Picture B).

1.2.1.3. Recrystallization

Recrystallization involves changing the size of crystals of a figured element, matrix, or cement. This phenomenon has been observed in some samples by completely erasing the walls or structures of the bioclasts (refer to Board I, Picture F).

1.2.1.4. Pyrite Cementation

Pyrite, typically resulting from the epigenization of organic matter, is expressed in the analyzed samples in the form of tiny microcrystalline nodules highlighting fine millimeter laminations or small grains dispersed in the clay matrix **(**refer to Board II, Picture C).

1.2.1.5. Organic Matter

Organic matter is ubiquitous in all samples analyzed from Z-1 well cores. It appears black in color and is usually associated with clay, with its rate reaching up to 10% locally. (Fig 6)

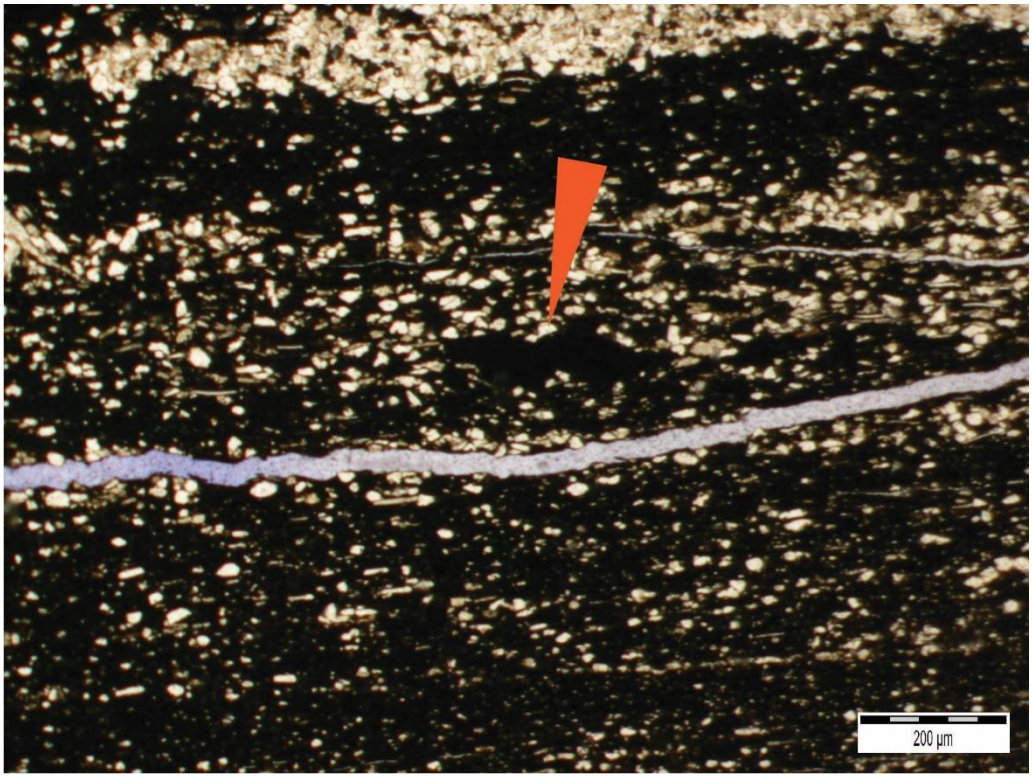

Figure 6: organic matter in well Z-1 (Depth 3658.34m)

1.2.Mineralogical analysis:

1.2.1. Diffraction X-Ray (XRD):

The mineralogical composition of Frasnian sediments from cores 01, 03, 05, 07, 08, 09, 10, and 11 of well Z-1 was analyzed using X-ray diffraction (XRD) techniques. The results, detailed in Table X, highlight the prevalence of clays, carbonates (calcite and dolomite), and quartz as the main constituents. Projection of these findings onto a histogram (Fig.7) indicates that the majority of samples exhibit clay-siliceous mudstone and mixed mudstone clay facies. Additionally, carbonate intervals were identified at depths of 3647m and 3671.15m.

depth	carot nuber	Non-clay minerals								clay minerals						Others				Σ
		quartz	Plagioclases	K-Feldspaths	Calcite	Dolomite	Ankerite	Siderite	Total carbonates	Illite - Interstratified I/S	Micas	Kaolinite	Chlorite	Smectite	Total clays	Pyrite	Barite	Halite	Anatase	
3583.86	1	15.7	0.8		1.9	2.0		1.1	5.0	29.7	0.9	38.4			69.0	7.6			1.9	100
3586.08		13.5	0.7		0.6	1.8		1.9	4.3	32.5	1.2	39.8			73.5	6.9			1.1	100
3589.91		14.5	0.8		2.8	5.1		2.0	9.9	20.8	1.2	43.8			65.8	7.9			1.1	100
3595.34	3	15.9	0.7		2.7	3.8		1.6	8.1	21.9	1.4	41.5			64.8	8.9			1.6	100
3603.08		17.3	0.6		1.8	7.8	2.3	0.4	12.3	28.4	1.1	28.5			58.0	10.8			1.0	100
3607.33		16.5			3.4	3.0		0.4	6.8	28.0	1.1	37.9			67.0	8.9			0.8	100
3608.00		13.6			2.5	25.3	3.8		31.6	20.9		22.4			43.3	10.8			0.7	100
3610.75		25.1	0.5		8.0	1.0			9.0	24.4	0.8	22.6			47.8	17.1			0.5	100
3615.76	5	13.2			4.4	5.1	8.1		17.6	25.8		29.2			55.0	13.6			0.6	100
3619.56		14.5	0.6		1.1	5.8	2.4	0.4	9.7	31.0	1.1	31.5			63.6	10.5			1.1	100
3625.23		17.7			1.8			0.4	2.2	34.6	1.0	26.9			62.5	16.9			0.7	100
3628.40		14.4			2.6	0.3		0.3	3.2	29.8	0.9	36.8			67.5	13.6			1.3	100
3631.21		16.0	0.5		0.6			0.3	0.9	33.2	1.5	31.7			66.4	15.2	0.4		0.6	100
3639.45	7	18.3			5.4	5.9	2.1	0.3	13.7	28.0		26.1			54.1	13.1			0.8	100
3643.52		19.4			0.9	0.3		0.2	1.4	29.1	0.9	32.6			62.6	15.8			0.8	100
3647.00		5.1			73.6	3.5	1.2		78.3	8.1		4.6			12.7	3.9				100
3649.65		19.0			2.3	0.7		0.2	3.2	31.4	1.5	29.8			62.7	13.6	0.5		1.0	100
3654.67	8	16.8			7.8	1.5	6.9	0.3	16.5	27.8	1.1	22.2			51.1	14.1	0.7		0.8	100
3658.34	9	33.2	0.4		14.5			0.5	15.0	24.1	1.5	11.7			37.3	12.8	0.7		0.6	100
3663.80	10	23.0	0.5		6.8	0.6		0.4	7.8	33.1	1.6	20.0			54.7	12.8	0.6		0.6	100
3667.79		20.0	0.5		1.1	13.0	3.4	0.5	18.0	26.3	1.3	21.9			49.5	10.9	0.4		0.7	100
3671.15	11	2.6	0.7		94.6				94.6	1.0					1.0	1.1				100

Table: Mineralogical analysis results by X-ray diffraction of well Z-1 / 2019

Figure 7: Mineralogical variation profile as a function of well depth

1.2.2. The mineralogical composition:

In our investigation, we analyzed twenty-two (22) core samples from well Z-1 to determine the mineralogical composition. By projecting the percentages of clay minerals, quartz (both detrital and authigenic), and carbonates (calcite and dolomite) onto a ternary diagram (Fig. 8), we categorized them into distinct facies. The diagram revealed a predominant siliceous clay-rich facies, identified as "Silica-rich argillaceous mudstone," alongside other facies such as "Clay dominated lithotype," "Carbonate rich argillaceous mudstone," "Mixed argillaceous mudstone," and "Carbonate dominated lithotype."

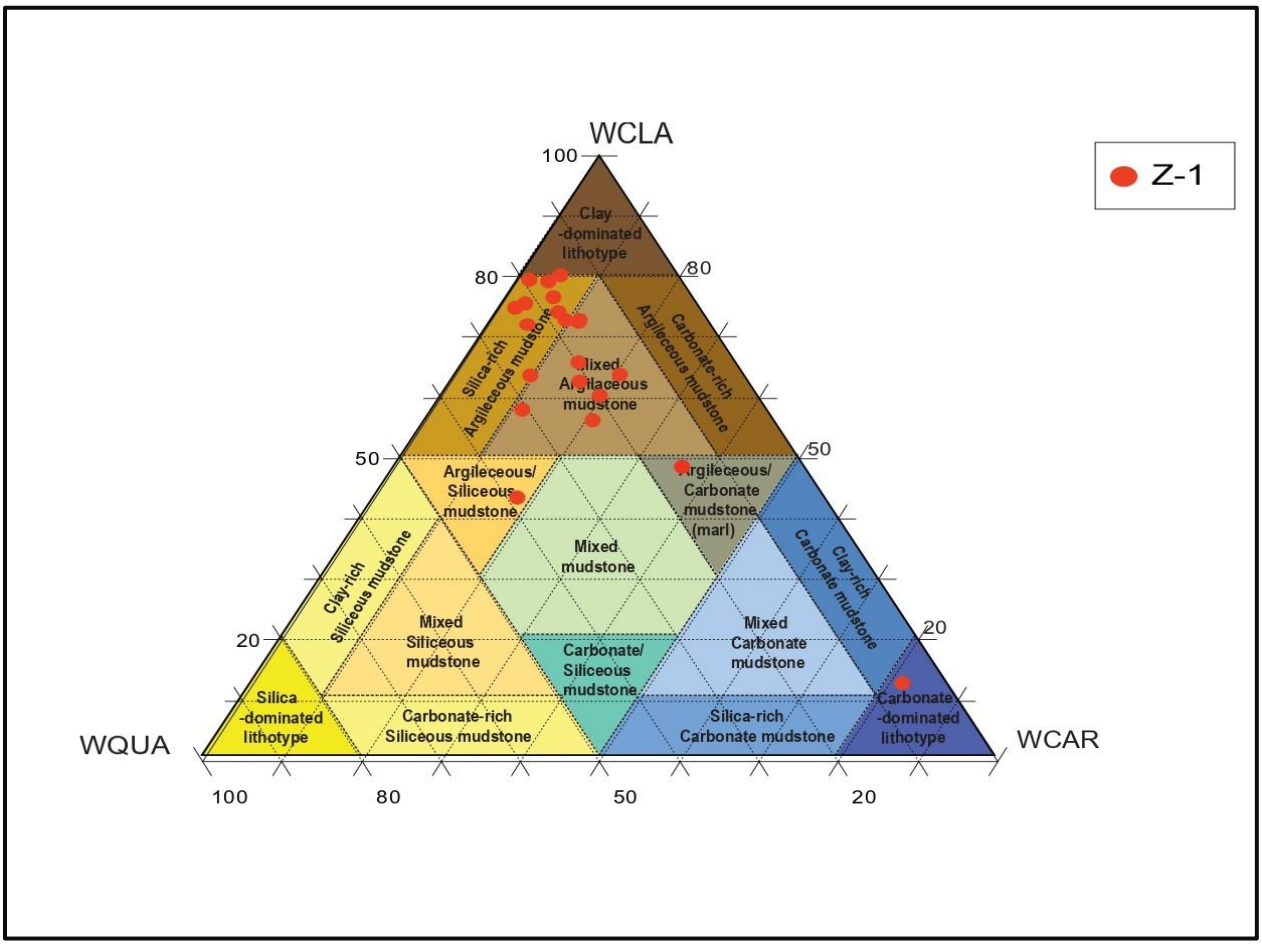

Figure 8: Teneray diagram of minerals observed within the Frasnian source rock

1.3.Petrography:

1.3.1. Scanning Electron Microscope (SEM) Analysis:

Twenty-two (22) samples from cores 01, 03, 05, 07, 08, 09, 10, and 11 of well Z-1 were subjected to Scanning Electron Microscope (SEM) analysis. The observations from this analysis are summarized below for select samples:

1.3.1.1. Sample: 3583.86m

- The sample predominantly consists of laminated clays with carbonate presence primarily in the form of calcite rods and crystals, alongside ankerite, siderite, and quartz crystals.
- Organic matter, plagioclases, apatite, and pyrite are also observed, with pyrite present in abundant framboïdal or small cubic crystal forms. (refer to Borad I, Picture C)

1.3.1.2.Sample: 3603.08m

- Carbonate crystals and clays dominate this sample, with dolomite being the main carbonate in rhombohedral crystal form, along with occasional calcite and ankerite.
- Quartz, organic matter, plagioclases, and pyrite are also present, with pyrite observed in framboïdal and small cubic crystal forms. (refer to Borad I, Picture B)

1.3.1.3.Sample: 3608.00m

- Abundance of carbonate crystals, predominantly rhombohedral dolomite, is observed along with clays.
- Quartz, apatite, and pyrite are also present, along with a minor presence of granite growth.
- The quartz content is approximately 15%, with 7% pyrite, 25% dolomites, 2% calcite, 4% ankerite, and 47% clay**.** (refer to Borad I, Picture C)

1.3.1.4.Sample: 3610.74m

- Carbonates and clays dominate this sample, with calcite being the main carbonate, occasionally accompanied by dolomite.
- Quartz, organic matter, apatite, anatase, sphalerite, and pyrite are also observed in various forms.(refer to Board I, Picture D)

1.3.1.5.Sample: 3615.76m

- Carbonates and clays are predominant, with calcite and dolomite being the main carbonate minerals.
- Quartz, organic matter, plagioclases, and pyrite are also present in various forms. (refer to Borad I, Picture E)

1.3.1.6.Sample: 3619.65m

- Clay predominates in this sample, with carbonate represented by dolomite, calcite, and ankerite.
- Quartz, organic matter, apatite, anatase, and pyrite are also observed.(refer to Borad I, Picture F)

1.3.1.7.Sample: 3628.4m

- Clay abundance suggests calm sedimentation conditions, with quartz grains showing heterogeneity in size and shape.
- Silica-filled laminations and styoliths indicate active diagenetic processes, alongside minerals like quartz, calcite, dolomite, pyrite, and anatase. (refer to Borad II, Picture A ,B ,C)

1.3.1.8.Sample: 3658.34m

- The sample exhibits alternation between silty clay, clay-dominated, and quartz and carbonate-dominated sections.
- Quartz, calcite, plagioclases, pyrite, and organic matter are observed, with quartz and calcite crystals varying in size. (refer to Borad II, Picture E)

1.3.1.9.Sample: 3671.15m

- Carbonate presence is primarily represented by calcite, with clays filling the pores.
- Quartz grains, plagioclases, organic matter, and traces of pyrite are also noted. (refer to Borad II, Picture F)

Board I

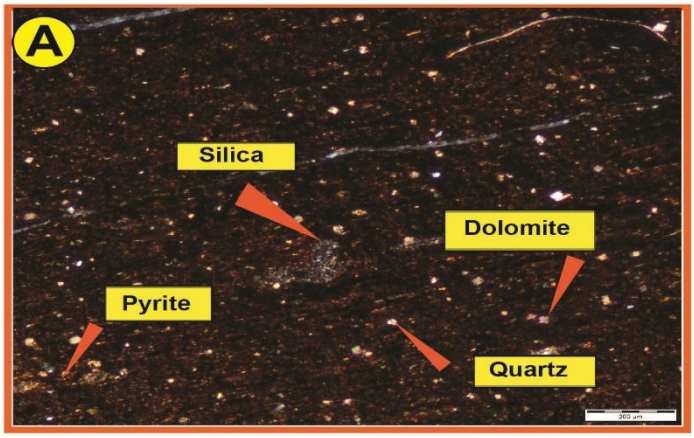

*well: **Z-1**, Alt: 3586,08m (LP) -Fransian*

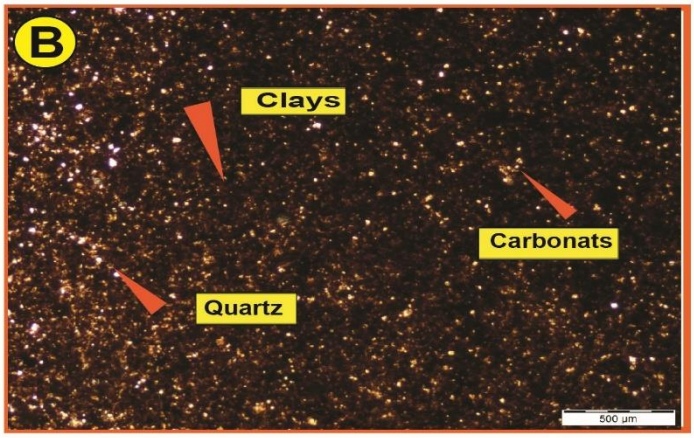

*well: **Z-1**, Alt: 3603,08m (LP)-Fransian*

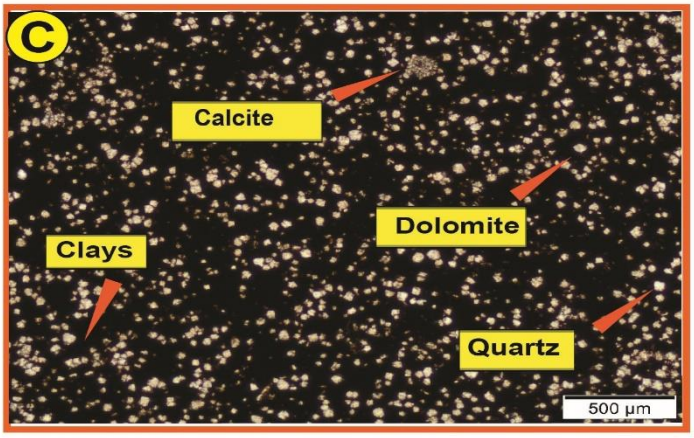

*well: **Z1**, Alt: 3608m (LN) -Frasnian*

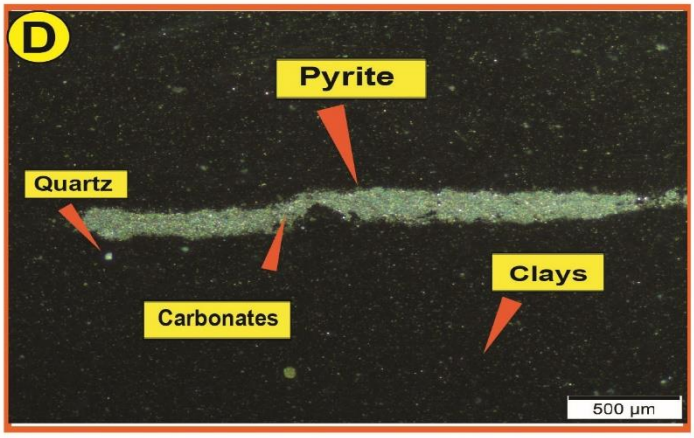

*well: **Z1**, Alt: 3610,74m (LP) -Frasnian*

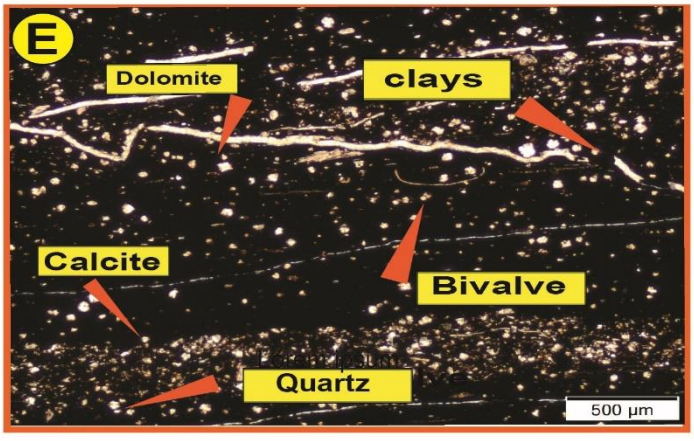

*well: **Z1**, Alt: 3615,74m (LN)-Frasnian*

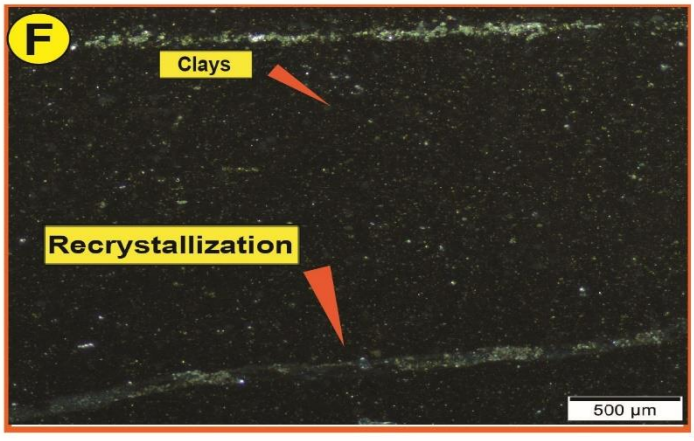

*well: **Z1**, Alt: 3619,76m (LP) - Frasnian*

Picture A : Dominance of clay , crystals dominate carbonates, accompanied by quartz crystals .
Picture B: Carbonates mainly comprise calcite ,with small-sized quartz crystals and clay minerals.
Picture C : Carbonates mainly comprise rhombohedral dolomite crystals,calcite,with small-sized quartz crystals and clay mineral.
Picture D : Carbonates and clays, with quartz of various sizes,pyrite .
Picture E : Carbonates and clays, mainly calcite and dolomite, with small quartz crystals , bivalve.
Picture F: Clays dominante ,recrystallization .

Board II

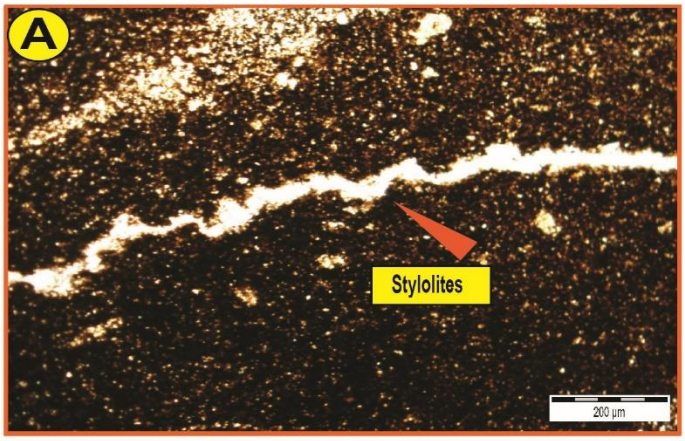

*Well: **Z-1**, Alt: 3628.4m (LN) -Frasnian*

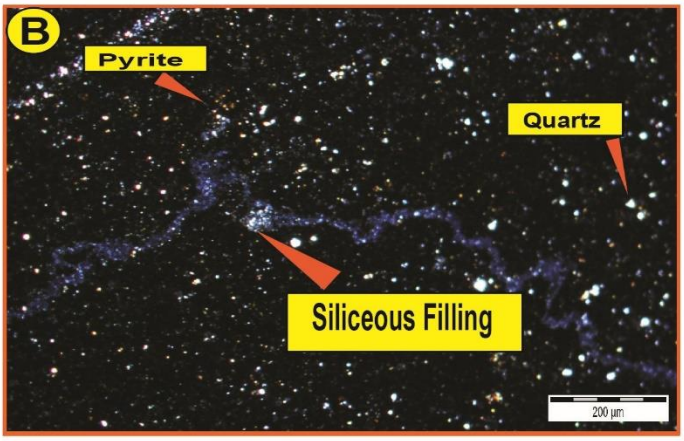

*Well: **Z-1**, Alt: 3628.4m (LP) -Frasnian*

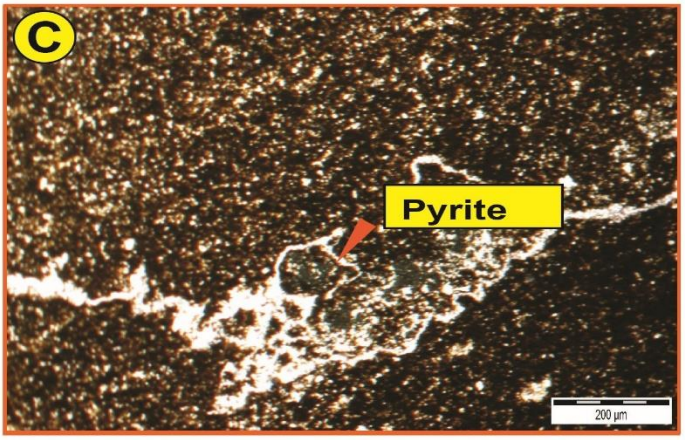

*Well: **Z-1**, Alt: 3628.4m (LNR) -Frasnian*

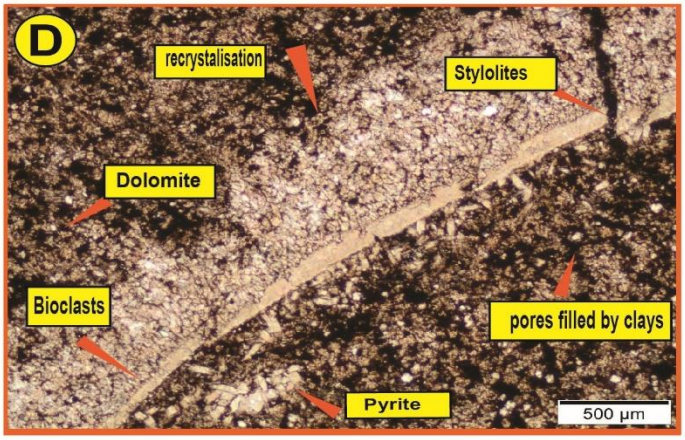

*Well : **Z-1**, Alt: 3647m (LN) - Frasnian*

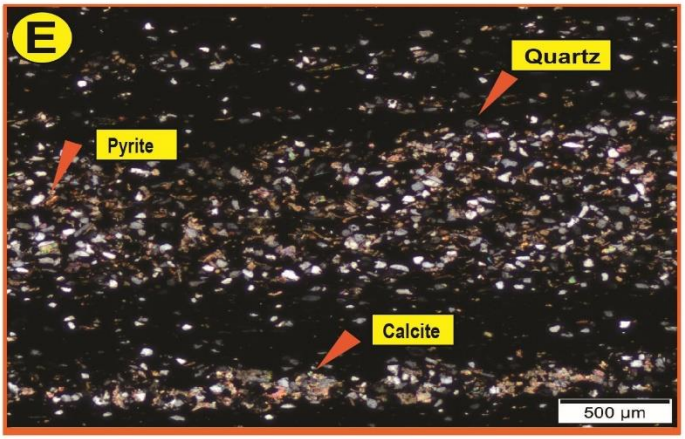

*Well: **Z-1**, Alt: 3658,34m (LP) -frasnian*

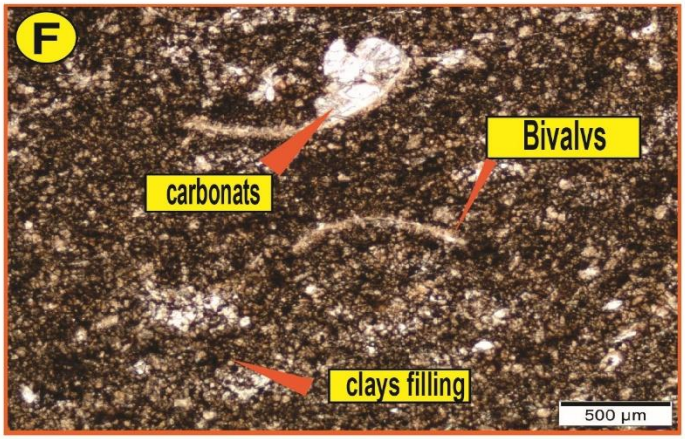

*Well: **Z-1**, Alt: 3671,15m (LN) - Frasnian*

Pictures A and B and C : Clays with quartz grains and stylolites filled with silicates,presence of pyrite
Picture D : Carbonates, primarily calcite with some dolomite crystals, accompanied by clays, small quartz crystals, rare plagioclases, and pyrite in various form .
Picture E : Silts alternate between clay and quartz dominance, with carbonates. Clay areas contain small quartz, calcite, and pyrite; quartz areas, larger crystals.
Picture F : Calcite carbonate with clay filling pores, along with quartz grains, and traces of raspberry-shaped pyrite ,bivalves.

2. Conclusion:

The comprehensive analysis of cores 01 to 11 from well Z-1, coupled with petrographic and mineralogical investigations, provides valuable insights into the depositional environment and diagenetic history of the Frasnian deposits. The findings suggest that these deposits originated in a distal marine platform setting characterized by anoxic conditions and low-energy hydrodynamics.

Based on the Ternary diagram, five lithofacies associations were identified, including clay-dominated lithotype, carbonate-rich argillaceous mudstone, mixed argillaceous mudstone containing clay, quartz, and carbonates, carbonate-dominated lithotype, and silica-rich argillaceous mudstone, as indicated by mineralogical analyses.

Scanning Electron Microscope (SEM) analyses corroborated the petrographic characteristics of these lithofacies, confirming the dominance of clay and carbonates with varying quartz content.

Petrographically, the Frasnian sediments are primarily composed of clay and carbonates, with quartz present in smaller proportions. Diagenetic processes observed include carbonate cementation, silicification, recrystallization of bioclasts, and pyrite cementation, all of which have impacted reservoir qualities to varying degrees.

Mineralogically, the main constituents of the Frasnian sediments are clays such as kaolinite, illite, and illite-smectite (I/S) interlayers, along with carbonates primarily composed of calcite and dolomite.

CHAPTRE 4: Geochemical evaluation of the Frasnian Source rock

CHAPTER 4: Geochemical evaluation of the Frasnian source rock

1. Introduction:

Understanding the properties of source rocks involves a comprehensive geochemical assessment to determine crucial parameters. Geochemistry investigates the distribution of chemical elements in rocks and minerals, shedding light on their origins and behaviors during geological processes. This scientific discipline utilizes the principles of chemistry, focusing particularly on planetary formation processes.

1.1. Pyrolysis Rock Eval:

Rock Eval pyrolysis entails subjecting a rock sample to high temperatures in an oxygen-free environment, leading to the release of gases and volatile organic liquids. These pyrolysis products undergo analysis to discern their chemical composition and physical attributes (Fig 9). Key parameters assessed include:

- Total organic matter content in the rock.
- Potential for oil and natural gas generation from the rock.
- Thermal maturity of organic matter, indicative of the age and geological conditions of rock formation.

Results from Rock Eval pyrolysis aid in estimating the quantity and quality of hydrocarbons within the rock, facilitating the assessment of oil or natural gas field production potential. The subsequent tables provide a summary of the geochemical analyses conducted on samples using Rock Eval 6 from well Z-1.

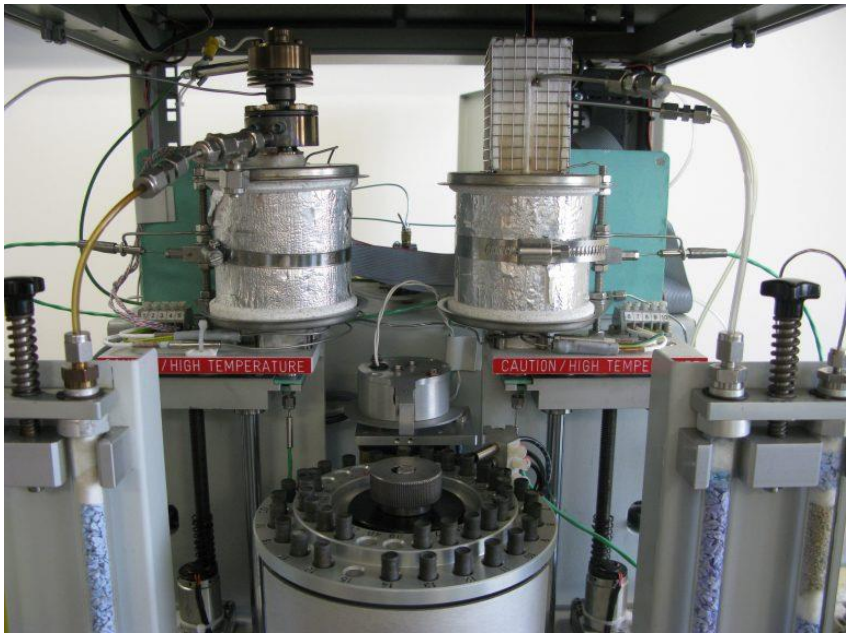

Figure 9: Rock-Eval 6 Turbo (ISTO 2021)

1.2. Total Organic Carbon (TOC)

Total organic carbon (TOC) content serves as a vital indicator of a source rock's oil potential. The TOC levels needed a rock to qualify as an oil source typically range from 0.5 to 1.5 wt%. Below 0.5 wt %, the rock is generally deemed poor or sterile in terms of oil generation potential. The table below illustrates the classification of TOC content based on richness in carbonate rock and clays.

Total Organic Carbon (TOC) %		Classification
Clay	Carbonates	
< 0.5	< 0.25	Poor
0.50 – 1.00	0.25 – 0.50	Fair
1.01 – 2.00	0.51 – 1.00	Good
2.01 – 4.00	1.01 – 2.00	Very good
> 0.04	> 2.00	Excellent

Table 5: Classification of rocks by organic carbon richness (Peter and Casa 1994)

1.3. Hydrogen IH and Oxygen IO

The hydrogen index (HI) and oxygen index (OI), often depicted on Van Krevelen diagrams, are valuable tools for the comprehensive characterization of organic matter and the elemental composition of kerogens.

The hydrogen index (HI) denotes the ratio of hydrogen to carbon in organic matter, while the oxygen index (OI) signifies the ratio of oxygen to carbon. They are calculated using the following formulas:

$$IO = \frac{100 * S3}{COT}$$

$$IH = \frac{100 * S2}{COT}$$

The table below summarizes the calculations for the hydrogen and oxygen indexes for well Z-1.

Depth (m)	TOC (%)	S1 (mg/g)	S2 (mg/g) avant lavage	IH (mg/g)	IP	Tmax	IO
3580.88	4.10	1.92	3.41	83	0.36	471	-
3680.78	1.46	0.71	0.93	64	0.43	481	-
3686.78	8.15	2.95	4.1	50	0.42	478	-
3691.78	11.97	3.32	6.71	56	0.33	480	-
3695.78	4.00	0.58	0.47	12	0.55	479	-
3702.78	3.99	1.38	1.42	36	0.49	481	-
3712.28	0.96	2.45	2.99	311	0.45	-	-
3722.28	5.72	2.38	2.39	42	0.50	481	-
3585.34	8.67	4.81	5.04	58	0.49	476	0
3586.64	8.78	6.65	5.20	59	0.56	477	0.46
3587.33	8.58	4.81	4.96	58	0.49	477	0.47
3588.86	5.98	3.86	3.08	52	0.56	476	0.50
3589.25	8.64	4.48	4.94	57	0.48	477	1.51
3591.33	8.32	4.48	5.17	62	0.46	477	1.44
3592.69	5.71	4.94	4.20	74	0.54	478	0.70
3593.28	8.60	4.79	5.18	60	0.48	476	1.28
3595.18	8.33	5.08	5.36	64	0.49	476	1.32
3597.28	8.69	4.33	5.15	59	0.46	475	0.92
3598.12	6.82	6	4.00	59	0.60	476	0.59
3599.23	8.40	4.87	4.99	59	0.49	476	0.36
3601.26	8.27	4.6	5.11	62	0.47	473	0.36
3603.28	9.55	5.27	5.36	56	0.50	472	0.42
3605.26	9.31	5.28	5.32	57	0.50	473	0.54
3605.86	9.68	3.62	4.31	45	0.46	473	0.31
3607.35	10.03	5.02	5.36	53	0.48	474	0.60
3609.38	9.77	4.57	5.39	55	0.46	474	0.72
3610.11	8.69	3.35	4.28	49	0.44	473	0.23

3611.23	9.51	4.93	5.51	58	0.47	469	0.63
3613.26	10.30	4.91	5.31	52	0.48	475	0.68
3613.53	10.94	5.3	5.13	47	0.51	471	0.18
3614.39	9.48	5.03	5.30	56	0.49	472	0.74
3617.48	9.39	5.06	5.34	57	0.49	474	0.75
3617.67	9.55	7.42	5.08	53	0.59	473	0.21
3619.38	9.55	4.82	5.34	56	0.47	473	0.63
3621.36	9.62	5.1	5.48	57	0.48	473	0.73

Depth (m)	**TOC (%)**	**S1 (mg/g)**	**S2 (mg/g) avant lavage**	**IH (mg/g)**	**IP**	**Tmax**	**IO**
3621.47	6.42	4.77	3.15	49	0.60	472	0.62
3623.36	12.15	5.02	5.46	45	0.48	475	0.49
3625.41	16.53	5.32	5.54	34	0.49	473	0.36
3627.14	8.44	5.75	4.32	51	0.57	472	0.24
3627.38	5.25	4.59	5.20	99	0.47	473	1.33
3629.41	9.29	4.99	5.39	58	0.48	474	0.65
3630.31	8.87	6.12	4.26	48	0.59	472	0.45
3631.38	11.14	6.41	5.10	46	0.56	472	0.63
3633.12	6.35	5.85	3.91	62	0.60	470	0.31
3633.34	10.13	6.68	5.09	50	0.57	472	0.69
3635.34	10.16	5.99	4.94	49	0.55	471	0.69
3638.36	10.00	8.58	5.49	55	0.61	475	0.90
3640.34	9.05	6.22	5.20	57	0.54	474	0.77
3641.36	8.63	8.02	4.96	57	0.62	474	0.46
3642.31	11.61	7.15	6.22	54	0.53	477	0.60
3644.3	9.95	7.39	6.04	61	0.55	477	0.70
3645.43	8.98	8.69	4.64	52	0.65	470	0.22

3646.36	9.90	7.52	5.95	60	0.56	475	0.71
3648.37	11.72	7.37	6.12	52	0.55	476	0.60
3650.31	12.34	7.19	6.44	52	0.53	478	0.65
3651.56	10.03	6.91	5.15	51	0.57	477	0.30
3652.38	11.88	4.51	6.02	51	0.43	474	0.59
3654.41	12.77	5.31	6.07	48	0.47	474	0.63
3656.45	10.07	6	6.28	62	0.49	474	0.40
3656.58	10.48	4.39	8.80	84	0.33	458	0.38
3659.35	10.36	6.08	6.09	59	0.50	475	0.29
3660.25	11.41	6.94	4.83	42	0.59	479	0.35
3663.4	11.02	7.11	5.62	51	0.56	478	0.36
3665.71	11.87	7.59	5.37	45	0.59	480	0.25
3666.35	10.30	7.18	5.46	53	0.57	477	0.29
3668.44	7.81	7.48	5.30	68	0.59	478	0.26
3669.7	11.11	7.85	6.09	55	0.56	484	0.36
3670.31	7.72	7.71	5.26	68	0.59	477	0.39
3672.41	7.80	7.83	5.57	71	0.58	476	0.51
3673.06	1.18	2.51	0.46	39	0.85	465	3.39

Table 6: Results of calculations of Hydrogen (HI) and oxygen (OI) indexes

1.4. Microscopic analysis of organic matter:

Microscopic analysis plays a crucial role in identifying and characterizing organic components at a microscopic scale. This method allows for the differentiation of various types of organic matter present in geological samples.

Moreover, microscopic studies are instrumental in assessing the maturity of organic matter, a pivotal factor in hydrocarbon formation. By examining the temperature and pressure conditions to which organic matter has been exposed over time, it becomes possible to determine whether it has undergone transformation into oil, natural gas, or coal (Fig 10).

Microscopic studies of kerogen types often involve the utilization of a photometric microscope coupled with a spectrometer (Fig 11). This equipment enables the determination of sample maturity by measuring the reflectivity of the sample's surface (R0%)

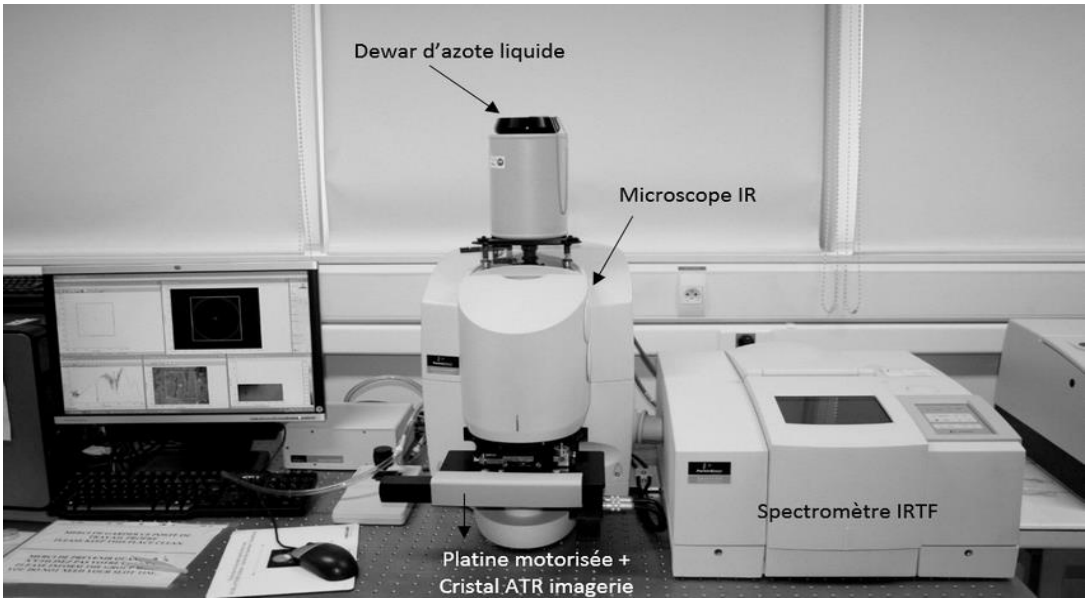

Figure 10: Photometric microscope coupled to a spectrometer (As and Co.)

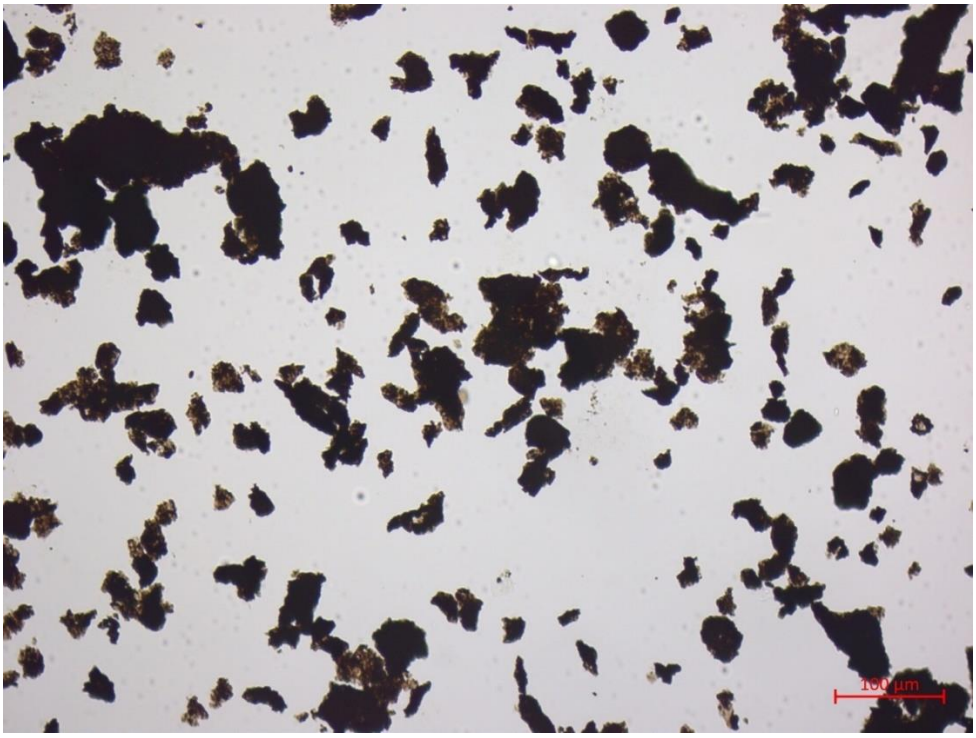

Figure 11: Example of organic matter observation (SONATRACH 2020)

1.5. Estimation of Hydrocarbon Volume in Shale Gas Source Rock:

The volume of hydrocarbons within the source rock can be estimated using key geochemical parameters such as oil potential (S1 + S2), total organic carbon content (TOC), and the volume of the source rock. This estimation method involves calculating the volume of the source rock and then multiplying it by the bulk density, TOC, and oil potential to derive an estimate of the reserves in place.

1.6. Correction of the adsorbed hydrocarbon Fraction:

Correcting for adsorbed hydrocarbons is crucial when estimating the volume of hydrocarbons from a source rock. Some hydrocarbons produced during the pyrolysis of organic matter can be adsorbed onto the surfaces of mineral particles within the source rock, reducing the estimated hydrocarbon volume available for production.

To address this adsorption phenomenon, thermal or chemical desorption methods are employed to recover the adsorbed hydrocarbons. Thermal desorption involves longer pyrolysis programs with

multiple temperature steps to release the adsorbed hydrocarbons. Chemical desorption methods utilize solvents to extract the adsorbed hydrocarbons, followed by reproducibility of the pyrolysis analysis to measure the adsorbed fraction by comparing the S2 parameters before and after washing**.**

1.7. Correction of Evaporated Loss:

Evaporation of free hydrocarbons in source rock samples can lead to loss. Various methods have been proposed to correct for this loss, including using the crude oil API density index and analyzing hydrocarbon content <15°C. Additionally, geochemical data can be utilized to calculate the amount of lost light hydrocarbons in S1 based on phase equilibrium and pyrolysis studies under different temperature and pressure conditions.

1.8. Mass to Volume Conversion:

Estimating the volume of hydrocarbons from source rocks involves converting mass to volume, as reserve estimates are typically expressed in volume units while geochemical parameters are measured in mass. The conversion factor depends on the density of the rock and the hydrocarbon component.

Density determination often requires laboratory analysis of fluid samples from the reservoir. In the absence of such analysis, empirical correlations can be used. Once density is determined, mass-to-volume conversion is conducted, which is crucial for accurate estimation of hydrocarbon volume. However, it is important to acknowledge that this conversion introduces uncertainty due to variations in rock and hydrocarbon density with depth and location

2. Geochemical evaluation of the Frasnian source rock

2.1. TOC Study

The measurement of Total Organic Carbon (TOC) provides insight into the overall organic carbon content within the Frasnian rock. This study was conducted for the well under investigation, and subsequently, a TOC variation profile was established as a function of depth.

Figure 12 depicts the distribution of TOC quantities relative to the depth of the bedrock in well Z-1

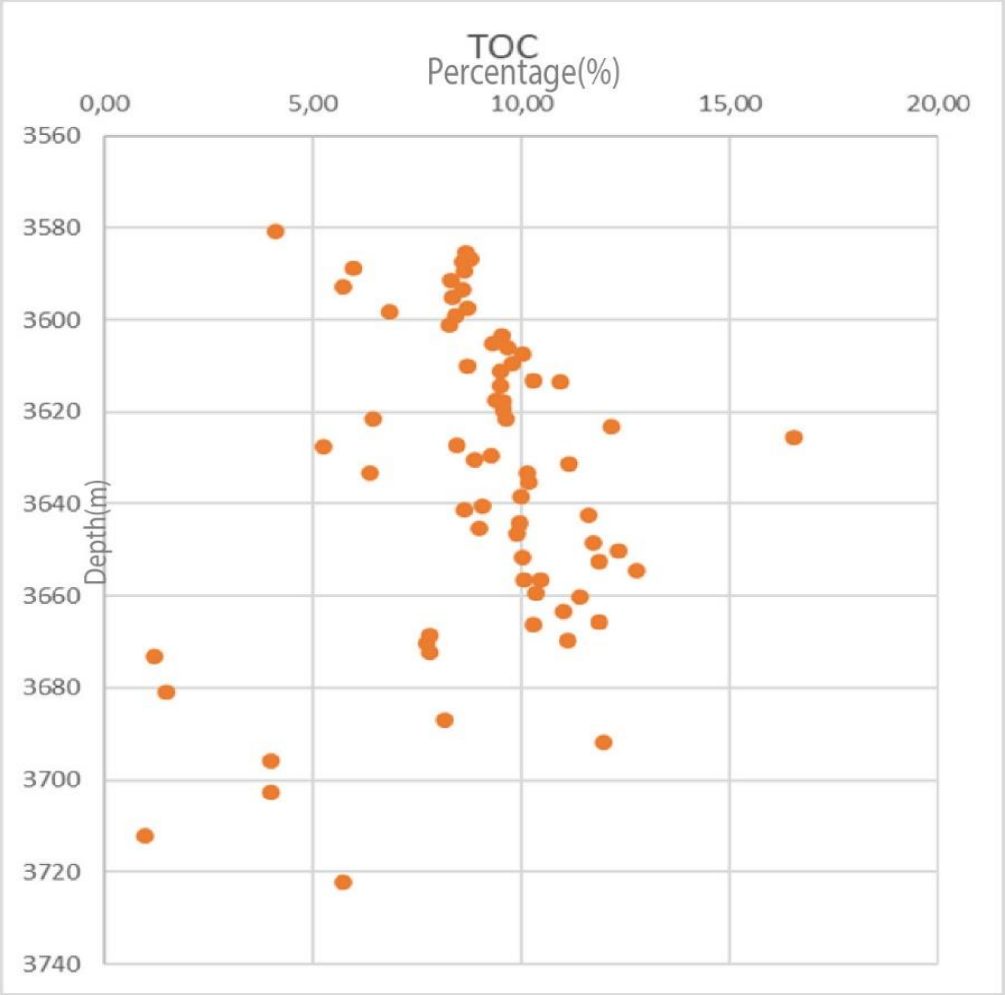

Figure 12: TOC variation profile as a function of depth in wells Z-1

The TOC variation profile, as a function of depth, reveals a subtle fluctuation in organic matter content throughout the well Z-1. The minimum value of 0.96% occurs at a depth of 3712.28 m, while the maximum value peaks at 16.53% around 3624.41 m. A consistent evolution is observed, punctuated by anomalies such as a significant increase between 3621.47 m and 3627.38 m. Conversely, there is a notable decrease in TOC between depths of 3672.41 m and 3680.78 m, followed by a gradual rise and another decline until it reaches the minimum at 0.96%.

Overall, the average TOC in well Z-1 is approximately 8.88%. According to the classification by Peter and Casa (1994), this TOC content falls within the "excellent" range (table 7), denoted by a rating of 4.

TOC %	Poor	Fair	Good	Very good	Excellent
Clay	< 0.5	0.5 – 1	1 – 2	2 – 4	4 >
Average TOC analyzed	-	-	-		8.88

Table 7: Classification of the amount of TOC in well Z-1 from Peter and Casa 1994.

2.2. Petroleum Potential

2.2.1. Free Potential S1

The free potential (S1), measured in milligrams of hydrocarbons per gram of rock (mg HC/g), was evaluated for both study wells. The obtained results were utilized to construct a depth-wise profile illustrating the variation of this parameter (Fig 13).

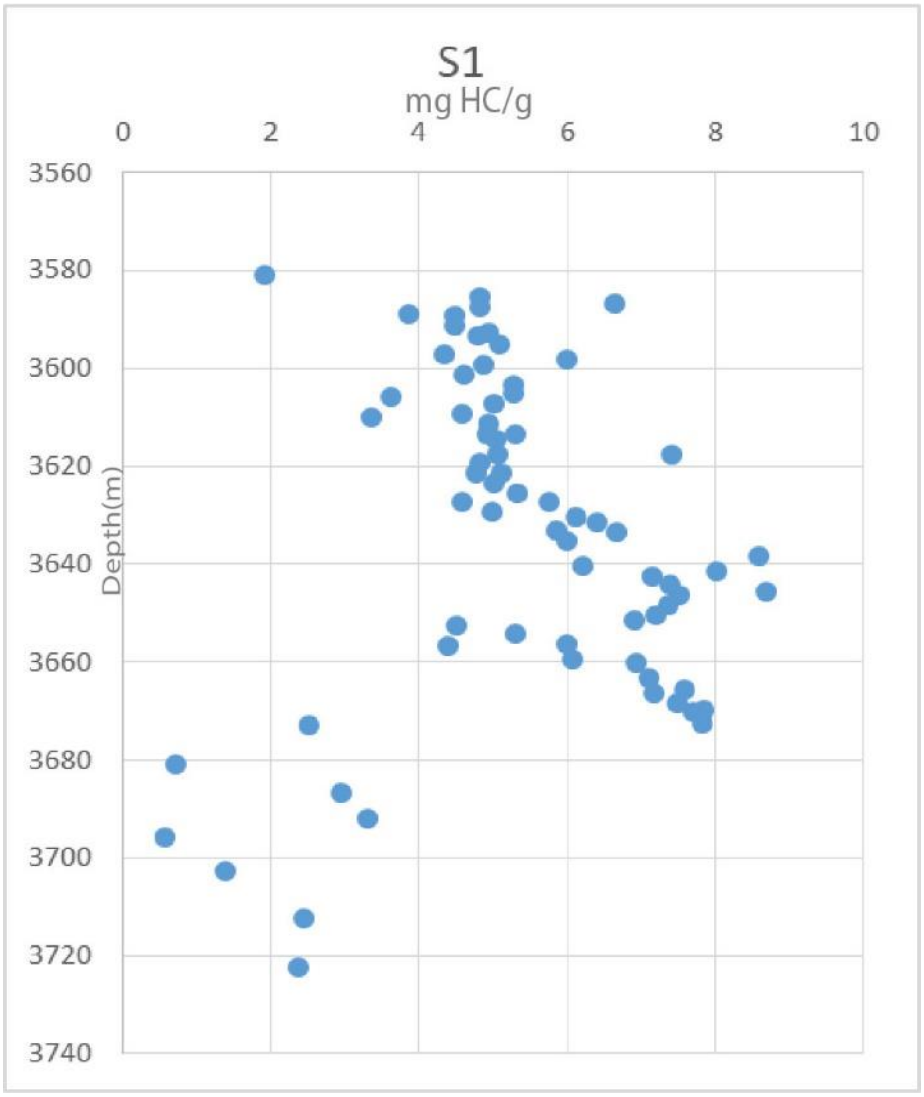

Figure 13: Free potential variation profile S1 as a function of depth in the well Z-1

In well Z-1, the pattern of variation of the free potential (S1) with depth reveals an average value of 5.34 mg HC/g. The minimum value of 0.58 mg HC/g is observed at a depth of 3695.78m, while the maximum value of 8.69 mg HC/g is recorded at a depth of 3645.43m (table 8). Notably, there is a notable decrease in S1 within the interval 3680.78m-3702.78m. Overall, the free potential (S1) of well Z-1 is deemed excellent.

S1 mg HC/g	Poor	Fair	Good	Very good	Excellent
Classification	< 0.5	0.5 – 1	1 – 2	2 – 4	4>
Average of S1	-	-	-	-	5.34

Table 8: The Classification of the amount of S1 in well Z-1 according to Peter and Casa 1994.

2.2.2. Residual Potential S2

The residual potential (S2), expressed in mg of hydrocarbon per gram of rock (mg HC/g), was measured for both study wells. The results are utilized to construct a variation profile of this parameter as a function of depth. (Fig 14)

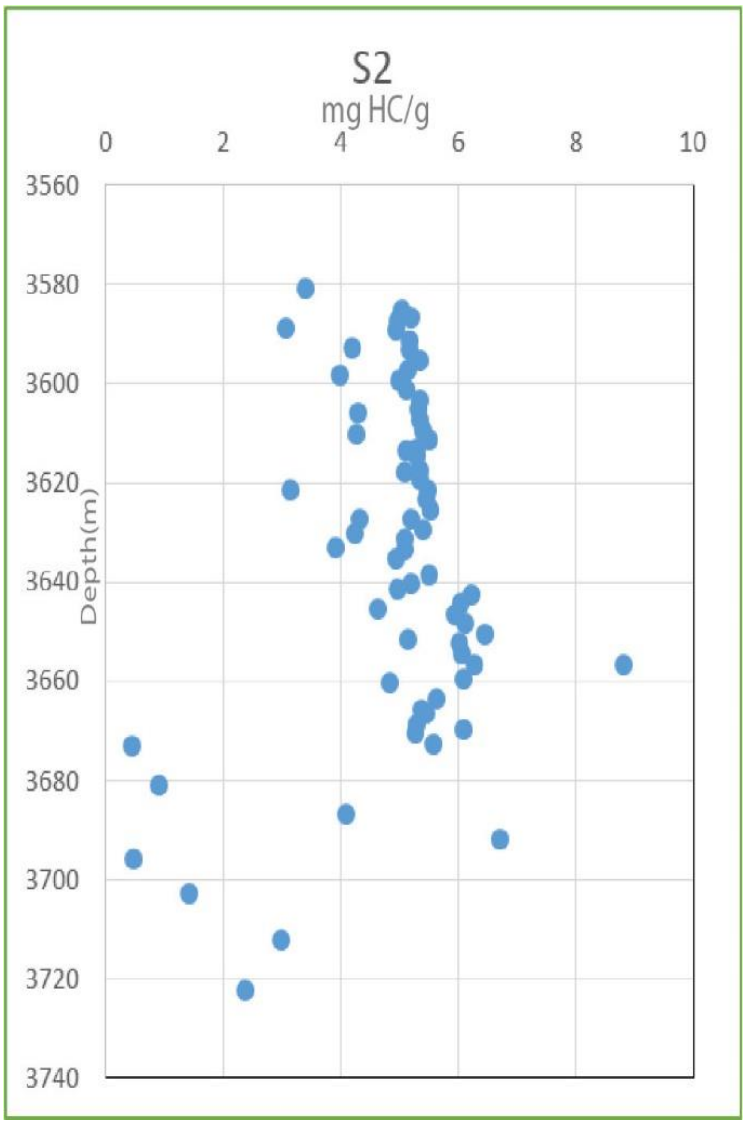

Figure 14: Profile of variation of residual potential S2 as a function of depth in the well Z-1

the variation pattern of the residual potential S2 as a function of depth in well Z-1 reveals an average value of 4.90 mg HC/g. The minimum value is recorded at 0.46 mg HC/g at a depth of 3673.06m, while the maximum value reaches 8.80 mg HC/g at a depth of 3656.58m (Table 9). According to the classification by Peter and Casa (1994), the S2 potential in well Z-1 is considered good.

S2 mg HC/g	Poor	Fair	Good	Very Good	Excellent
Classification	< 2.5	2.5 – 5	5 – 10	10 – 20	> 20
Average S2 analyzed	-	-	8.80	-	-

Table 9: The classification of the quantity of S2 in well according to Peter and Casa 1994.

2.3. Thermal Maturation

The thermal maturation diagram indicates the type of hydrocarbon maturation phase in the Frasnian source rock. Based on the measured vitrinite reflectance values (average Tmax = 474°C) and the corresponding IP values, it suggests that the kerogen is in the gas window (Fig 15). The observed Tmax values confirm that the kerogen is generating wet gas, indicating a very advanced stage of maturity where its potential for hydrocarbon production is nearly exhausted.

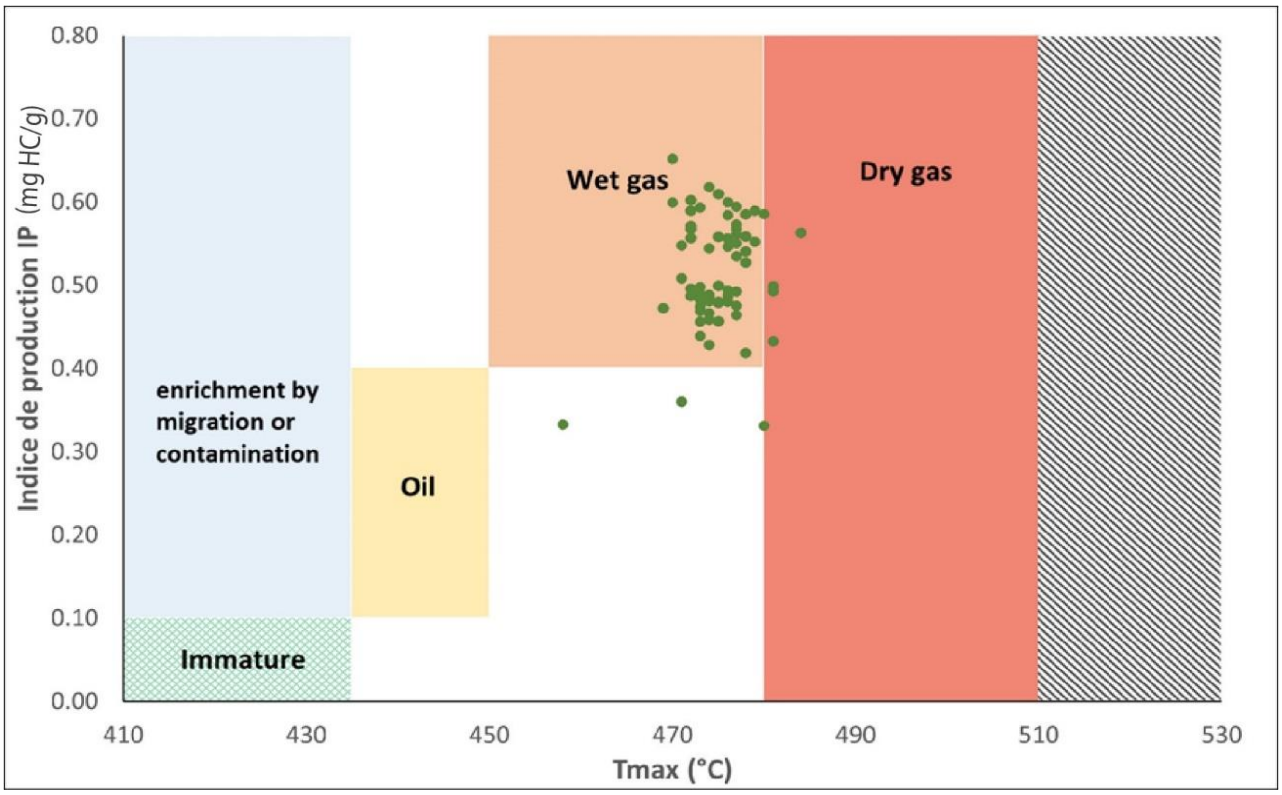

Figure 15: Maturation diagram according to IP and Tmax of Z-1 well.

2.4. The type of kerogen (Tissot diagram)

The HI vs. OI correlation diagram is used to determine the type of kerogen present in the Frasnian source rock. Additionally, a diagram correlating T-max and HI is employed to validate this information. However, the analysis reveals very low HI (mean = 59 mg/g) and OI (0.62 mg/g) values, making it challenging to determine the kerogen type. The points on the diagram suggest a distribution across the three kerogen types, although type 3 kerogen can be excluded due to extremely low IO values. Further analysis indicates advanced maturity, suggesting the presence of type 2 kerogen (Fig 16). However, the final confirmation of the kerogen type will be obtained through microscopic study

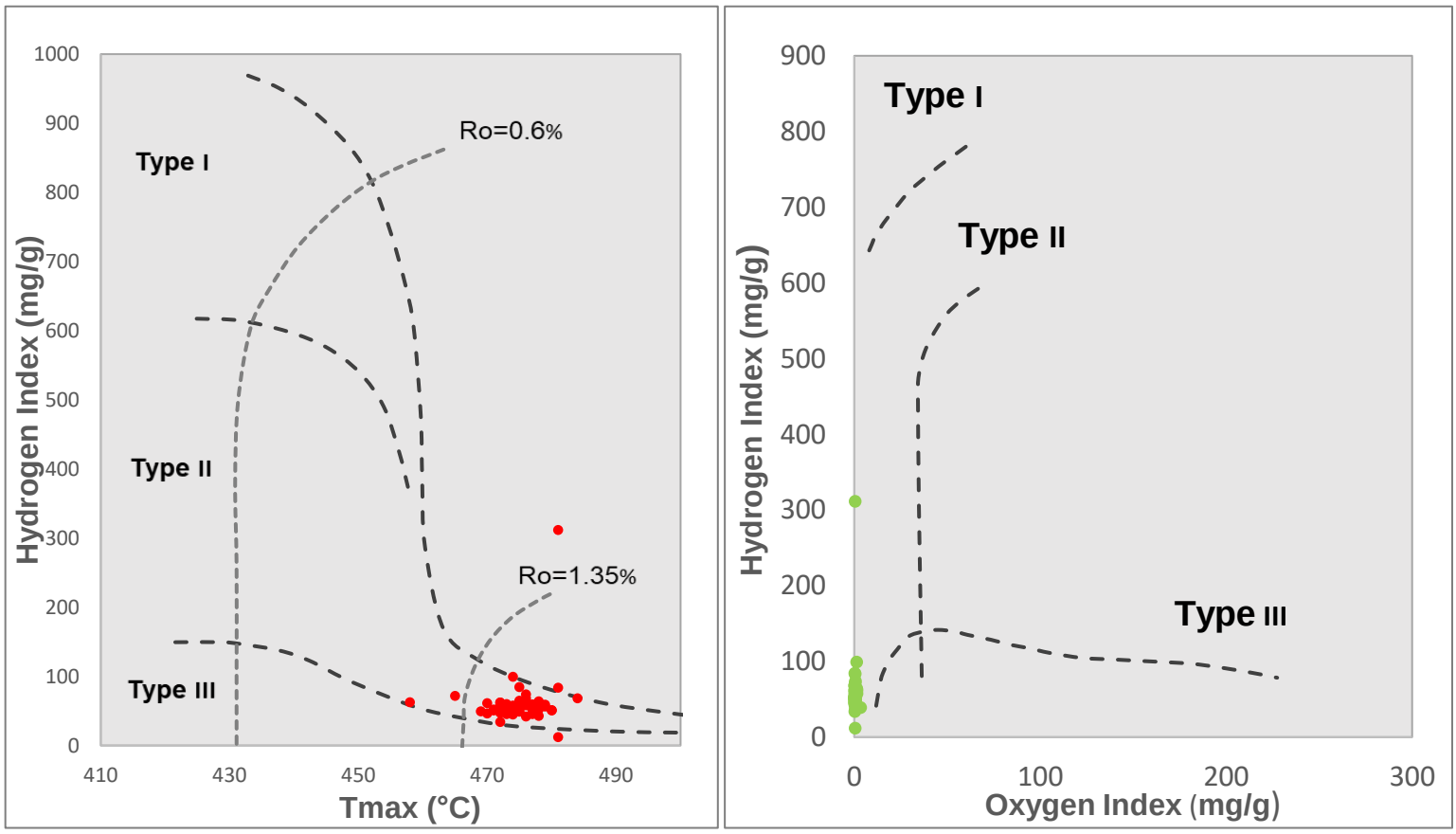

Figure 16: Diagram of the hydrogen index as a function of oxygen index and diagram of T-max HI showing different types of kerogens in the Frasnian source rock.

3. Microscopic study

Microscopic analysis is crucial for confirming hypotheses and gaining a deeper understanding of the composition and quality of kerogen in the wells. It helps to elucidate hydrocarbon formation processes and predict potential hydrocarbon production from these organic rocks.

In a microscopic study conducted for both Z-1 wells, images of the Frasnian source rock were analyzed. The organic matter in the core interval of the Frasnian in well Z-1 primarily appears amorphous, with minimal proportions of palynomorphs and phytoclasts. Under the microscope, organic matter exhibits weak alteration, with some components, particularly phytoclasts, being partially or entirely opaque. (Fig 17)

Based on this description, it can be concluded that the observed organic matter in the samples corresponds to **type II** kerogen, potentially transitioning from **type I** to **type II**, indicating high initial potential for hydrocarbon generation . (Fig 18)

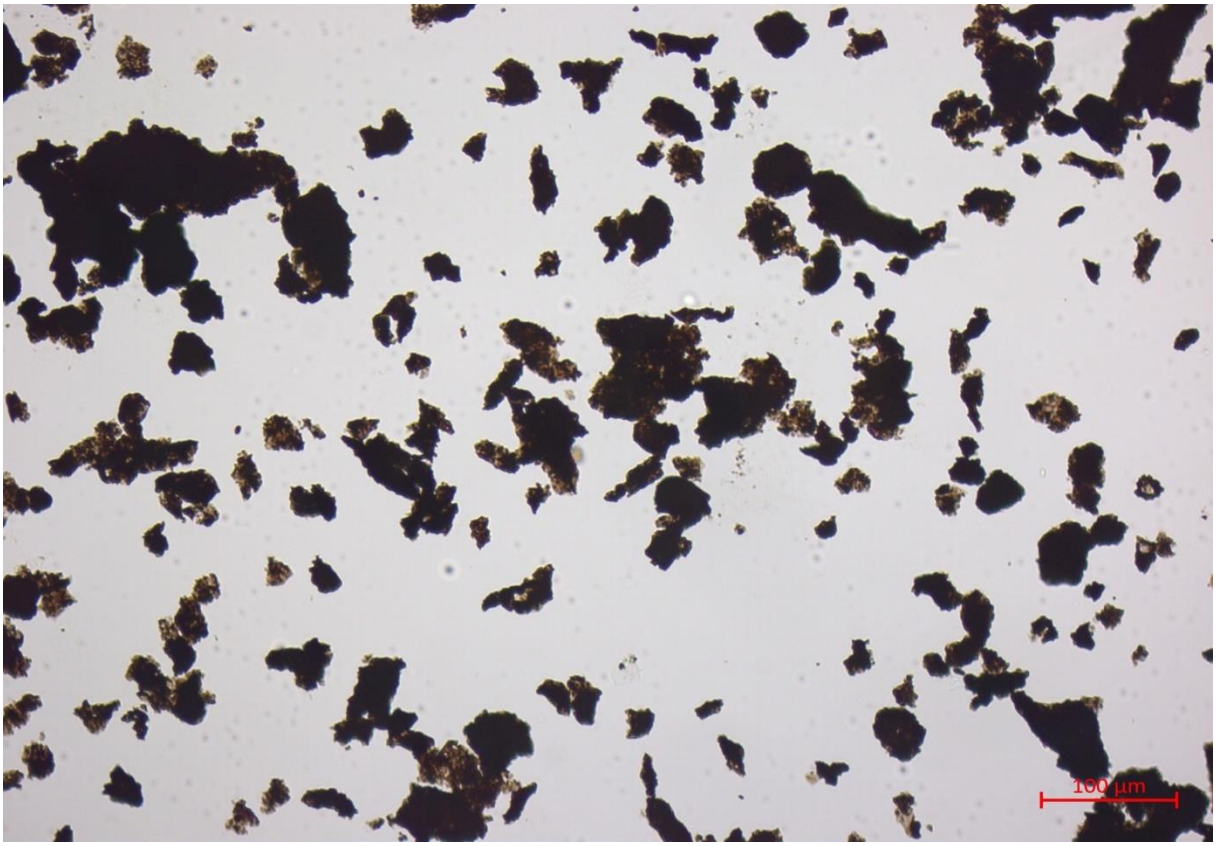

Figure 17: Microscopic photo of the organofacies of sample 3668.40m

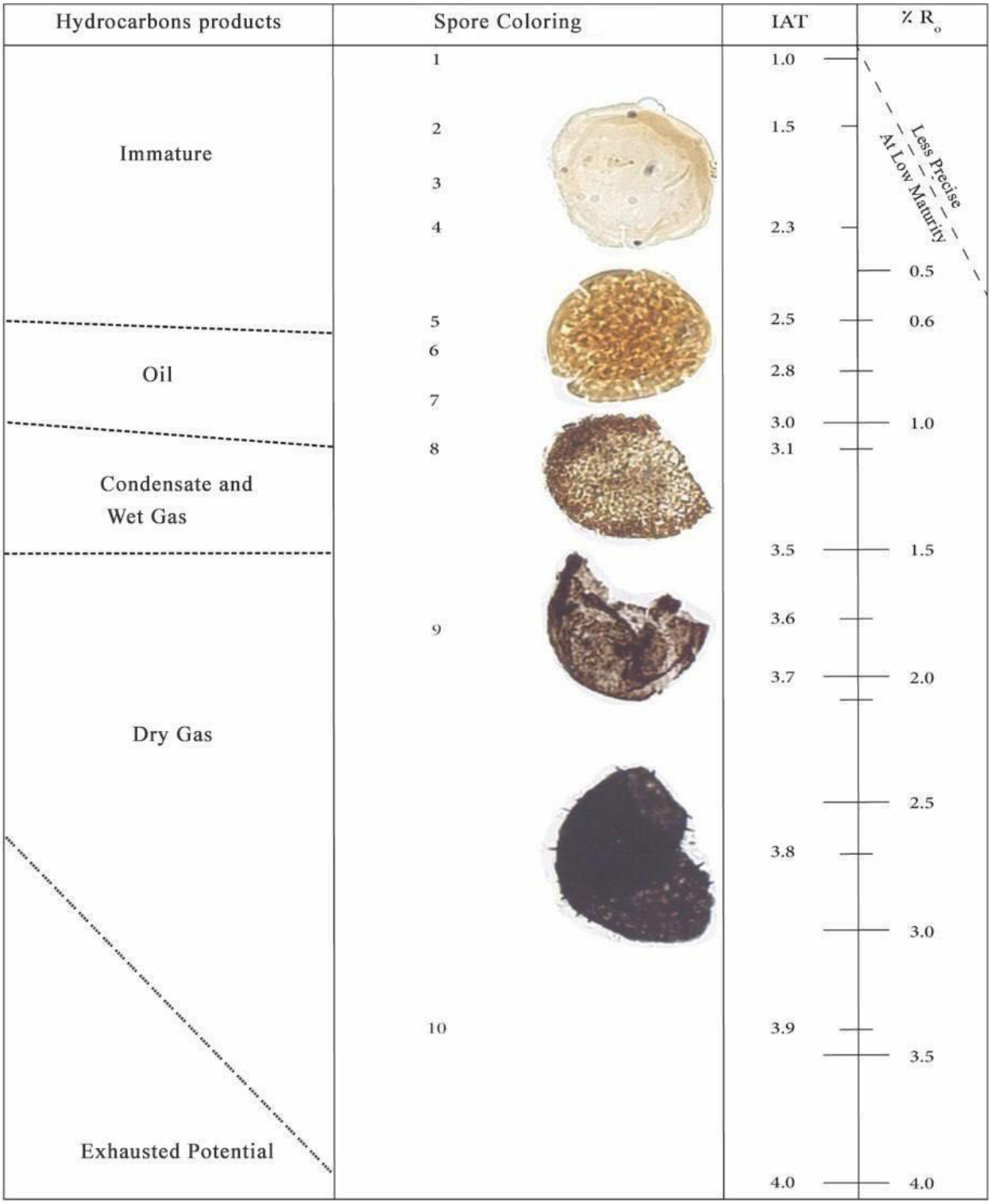

Figure 18: Maturity scales and hydrocarbon products (Marshel and Yule, 1999)

3.1. Thermal Alteration Index

The Thermal Alteration Index (TAI) serves as a maturity parameter, relying on the coloration of spores and other palynomorphs. Estimating TAI on samples from this well proved challenging due to the amorphization of kerogen, leaving few exploitable palynomorphs. However, with careful scrutiny, estimates were possible for most samples, yielding TAI values between **3.4** and **3.5**. This indicates a transition phase from wet to dry gas. (Fig 19).

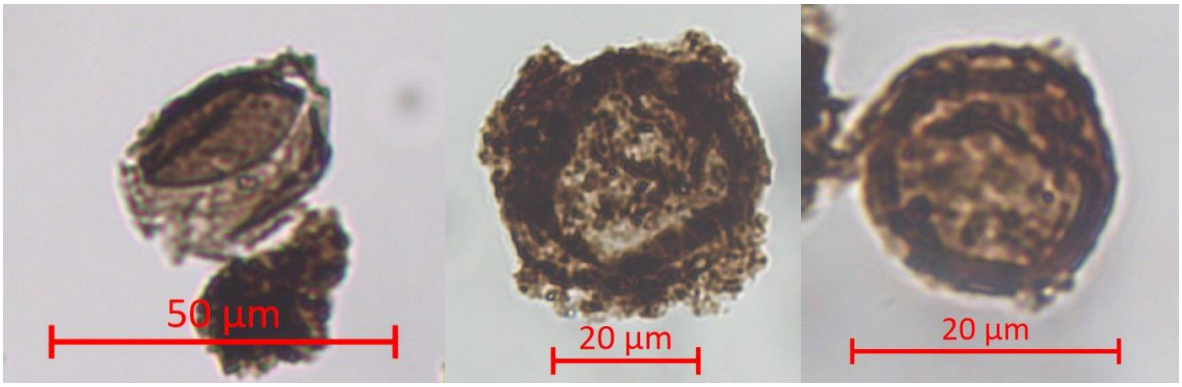

Sporomorphic alga alga

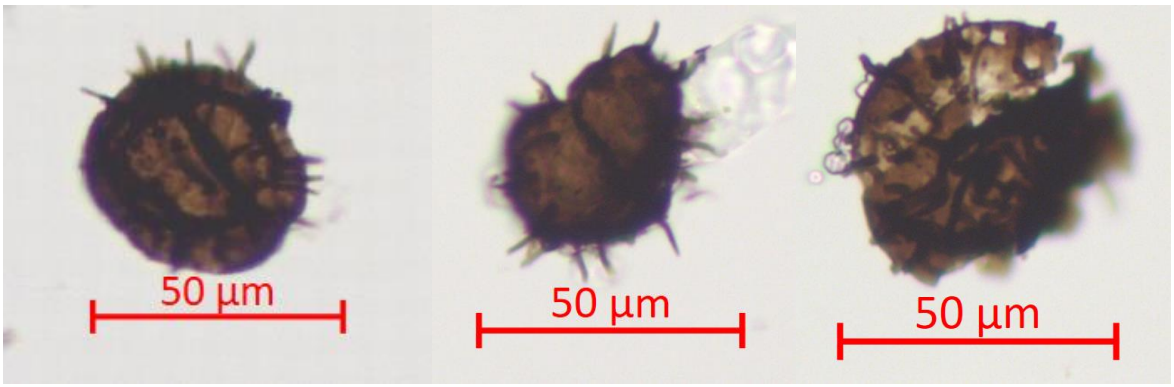

Acritarche acritarche acritarche

Figure 19: Some palynomorphs (algae and acritarches) of the carrot level used for the maturity estimate.

The summarized results in the table 10 suggest that the Frasnian core interval is at the cusp of concluding wet gas generation and commencing dry gas generation, with a TAI ranging from 3.4 to 3.5

Depth (m)	**TAI**	**Maturity**	**Alteration (opacity)**	**Initial potentiel**
3582.56	3.5	Dry gas start	Low	I – II
3602.48	N/A	N/A	Low	I – II
3623.50	3.4 – 3.5	End of wet gas / Dry gas start	Low	I – II
3644.45	N/A	N/A	Low	I – II
3668.40	3.5	Dry gas start	Low	I – II
3678	3.4-3.5	End of wet gas / Dry gas start	Low	II
3719.50	3.5	Dry gas start	Low	II

Table 10: Summary of the results of the micros and their maturity

4. Conclusion:

In conclusion, the study of the Frasnian source rock in well Z-1 has provided valuable insights into its composition and petroleum potential:

- The average Total Organic Carbon (TOC) content in well Z-1 is approximately 8.88%, classified as excellent according to Peter and Casa (1994).
- The Free Potential (S1) in well Z-1 exhibits an average value of 5.34 mg HC/g, indicating excellent potential for hydrocarbon production.
- The Residual Potential (S2) in well Z-1 shows an average value of 4.90 mg HC/g, classified as good potential for hydrocarbon generation.
- Thermal maturation analysis reveals that the kerogen in the Frasnian source rock is situated within the gas window, with an average Tmax of 474°C, signifying advanced maturity and wet gas generation.
- Analysis using the Tissot diagram indicates low Hydrogen Index (HI) and Oxygen Index (OI) values, suggesting advanced maturity and a probable type 2 kerogen.
- Microscopic examination reveals that the organic matter in the Frasnian source rock is predominantly amorphous, with minimal proportions of palynomorphs and phytoclasts, it appears to be sapropellique organic matter.
- The organic matter displays weak alteration, indicative of high initial potential, and is classified as type II.
- The Thermal Alteration Index (TAI) suggests a transition from wet to dry gas generation, with TAI values ranging between 3.4 and 3.5 for the Frasnian core interval.

Overall, these findings underscore the promising petroleum potential of the Frasnian source rock in well Z-1, highlighting its favorable characteristics for hydrocarbon exploration and production

CHAPTER 5: “Estimation of hydrocarbon volumes in the Frasnian source rock”

CHAPTER 5: Estimation of hydrocarbon volumes in the Frasnian source rock

1. Introduction

Estimating the volume of hydrocarbons within the source rock is crucial for assessing its potential for hydrocarbon extraction. This estimation relies on various geochemical parameters, including oil potential (S1 + S2) and total organic carbon (TOC), but adjustments are necessary to account for differences between sample conditions and in-situ conditions. In the case of well Z-1, both TOC and S1 values are notably high, indicating favorable conditions for hydrocarbon assessment.

2. Correction of adsorbed fraction

The correction of the adsorbed fraction is essential for accurately determining the actual quantity of hydrocarbons available for extraction from the source rock. This correction involves specific laboratory methods designed to separate adsorbed hydrocarbons from free ones. Pyrolysis analysis of S2 (before and after washing) allows for quantifying the contribution of adsorbed hydrocarbons. By comparing S2 with S2', the residual potential after washing, it becomes possible to assess the potential of extractable hydrocarbons more accurately, incorporating both free and adsorbed hydrocarbons. (Table 11).

The formula used for this calculation is:

$$S1' = S2 - S2'$$

, where

• S1’ represents the adsorbed fraction

• S2 stands for the residual potential

• S2’ denotes the residual potential after washing.

Depth(m)	S2 (mg/g) unwashed	S2 Washed	S1' (mg/g)	Depth(m)	S2 (mg/g) unwashed	S2 Washed	S1' (mg/g)
3580,88	3,41	2,22	1,19	3609,38	5,39	4,75	0,64
3680,78	0,93	0,76	0,17	3610,11	4,28	3,94	0,34
3686,78	4,1	2,79	1,31	3611,23	5,51	4,63	0,88
3691,78	6,71	4,39	2,32	3613,26	5,31	4,69	0,62
3695,78	0,47	0,39	0,08	3613,53	5,13	4,69	0,44
3702,78	1,42	1,17	0,25	3614,39	5,30	4,67	0,63
3712,28	2,99	0,25	2,74	3617,48	5,34	4,44	0,9
3722,28	2,39	1,18	1,21	3617,67	5,08	3,88	1,2
3585,34	5,04	4,27	0,77	3619,38	5,34	4,04	1,3
3586,64	5,20	4,63	0,57	3621,36	5,48	4,96	0,52
3587,33	4,96	4,26	0,7	3621,47	3,15	3,06	0,09
3588,86	3,08	2,79	0,29	3623,36	5,46	3,84	1,62
3589,25	4,94	4,83	0,11	3625,41	5,54	4,71	0,83
3591,33	5,17	4,46	0,71	3627,38	5,20	4,79	0,41
3592,69	4,20	3,68	0,52	3629,41	5,39	4,87	0,52
3593,28	5,18	4,43	0,75	3630,31	4,26	1,65	2,61
3595,18	5,36	4,57	0,79	3631,38	5,10	2,7	2,4
3597,28	5,15	4,03	1,12	3633,12	3,91	3,33	0,58
3598,12	4,00	3,61	0,39	3633,34	5,09	0,55	4,54
3599,23	4,99	4,38	0,61	3635,34	4,94	3,37	1,57
3601,26	5,11	4,48	0,63	3638,36	5,49	3,14	2,35
3603,28	5,36	4,81	0,55	3640,34	5,20	2,7	2,5
3605,26	5,32	4,74	0,58	3641,36	4,96	4,3	0,66
3605,86	4,31	3,97	0,34	3642,31	6,22	5,3	0,92
3607,35	5,36	4,78	0,58	3644,3	6,04	5,27	0,77

Table 11: Calculation of the numerical application of the adsorbed fraction

The variation profile of the adsorbed fraction as a function of depth reveals a significant quantity of absorbed hydrocarbons, particularly within the interval of 3620m to 3640m. This underscores the importance of accurately assessing the petroleum potential by accounting for these absorbed fractions (Fig 20).

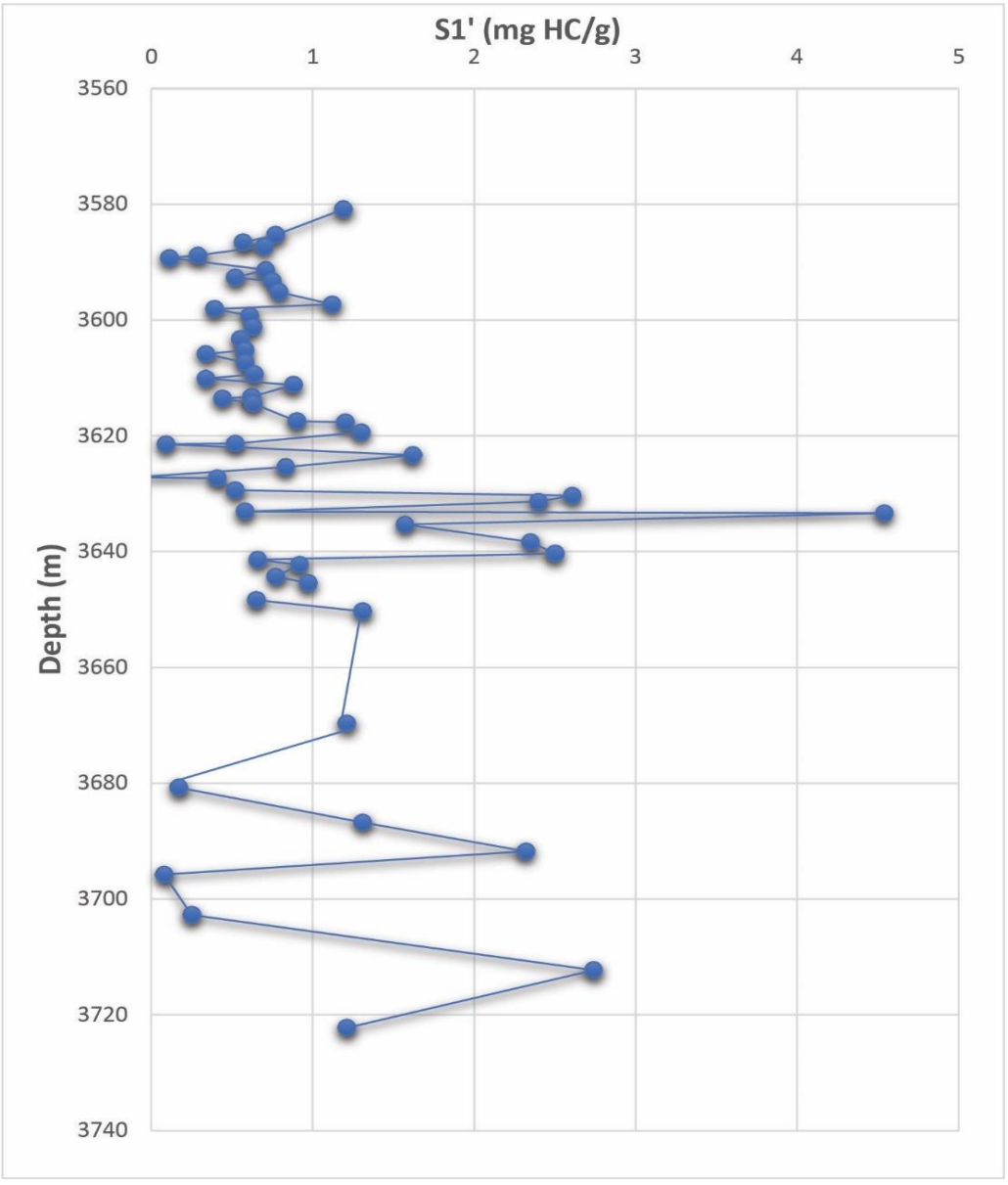

Figure 20: Variation profile of adsorbed fraction as a function of well depth Z-1.

3. Estimation of Evaporitic Loss

To estimate the loss of free hydrocarbons by evaporation, parameters such as crude oil API and hydrocarbon content below C15 are utilized in source rock samples. These parameters help gauge the amount of light hydrocarbons present in the samples and the oil potential of the source rock. In the case of the Frasnian source rock, characterized by a fine condensate ripening phase (474°C) and an API of 58, the evaporitic loss is calculated to be 65%.(Fig 21).

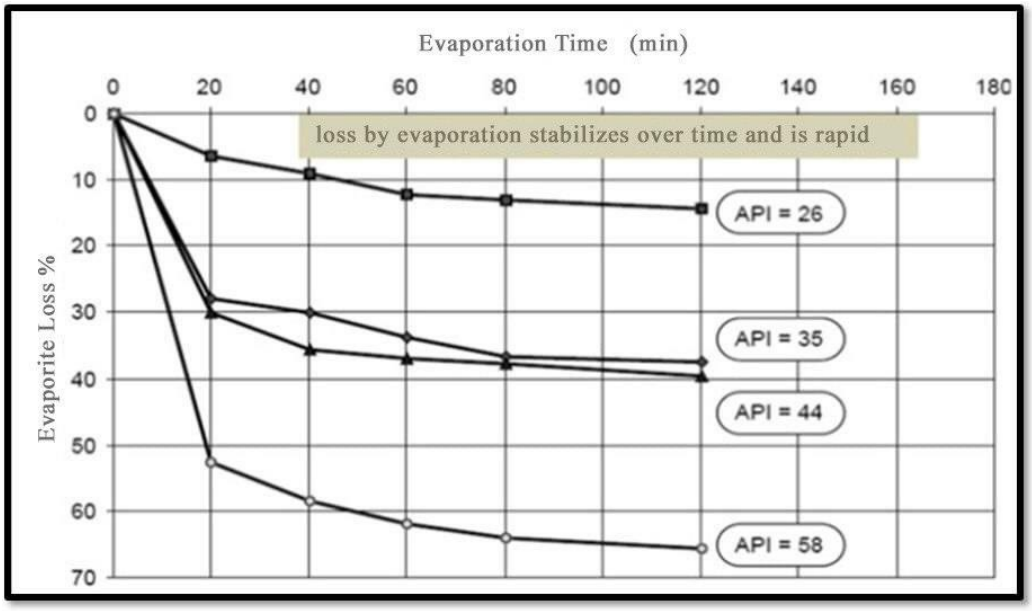

Figure 21: Graph shows the loss of hydrocarbons over time according to Noble R et al (1997)

According to Michael et al (2014), the assessment of free hydrocarbon loss by evaporation is expressed as follows:

$$HC\ loss = [(S1 + S1')\ \alpha]$$

with

• HC Loss: The Evaporitic Loss

• S1: Free Potential

• S1’ : The adsorbed fraction

• : The HC Loss correction coefficient

The correction of the Free Potential S1 is given by the formula S1*= HC loss + S1 + S1’ with

• S1*: Free Potential corrected

• HC loss: Evaporitic loss

• S1: Free Potential

• S1’ : The adsorbed fraction

The obtained results are summarized in table 12

Depth (m)	S1' (mg/g)	S1 (mg/g)	S1+S1'	HC Loss (mg/g)	S1* (mg/g)	Depth (m)	S1' (mg/g)	S1 (mg/g)	S1+S1'	HC Loss (mg/g)	S1* (mg/g)
3580,88	1.19	1.92	3.11	1.06	4.17	3621,47	0.09	4.77	4.86	1.65	6.51
3680,78	0.17	0.71	0.88	0.3	1.18	3623,36	1.62	5.02	6.64	2.25	8.9
3686,78	1.31	2.95	4.26	1.45	5.71	3625,41	0.83	5.32	6.15	2.09	8.24
3691,78	2.32	3.32	5.64	1.92	7.56	3627,14	0.09	5.75	5.66	1.92	7.58
3695,78	0.08	0.58	0.66	0.22	0.88	3627,38	0.41	4.59	5	1.7	6.7
3702,78	0.025	1.38	1.66	0.55	2.18	3629,41	0.52	4.99	5.51	1.87	7.38
3712,28	2.74	2.45	5.19	1.76	6.95	3630,31	2.61	6.12	8.73	2.97	11.70
3722,28	1.21	2.38	3.59	1.22	4.81	3631,38	2.4	6.41	8.81	3	11.80
3585,34	0.77	4.81	5.58	1.9	7.48	3633,12	0.58	5.85	6.43	2.19	8.61
3586,64	0.57	6.65	7.22	2.45	9.67	3633,34	4.54	6.68	11.22	3.81	15.03
3587,33	0.7	4.81	5.51	1.87	7.38	3635,34	1.57	5.99	7.56	2.57	10.13
3588,86	0.29	3.86	4.15	1.41	5.56	3638,36	2.35	8.58	10.93	3.71	14.64
3589,25	0.11	4.48	4.59	1.56	6.15	3640,34	2.5	6.22	8.72	2.96	11.68
3591,33	0.71	4.48	5.19	1.76	6.95	3641,36	0.66	8.02	8.68	2.95	11.63
3592,69	0.52	4.94	5.46	1.86	7.3	3642,31	0.92	7.15	8.07	2.74	10.81
3593,28	0.75	4.79	5.54	1.88	17.42	3644,3	0.77	7.39	8.16	2.77	10.93
3595,18	0.79	5.08	5.87	2	7.87	3645,43	0.97	8.69	9.66	3.28	12.94
3597,28	1.12	4.33	5.45	1.85	7.30	3646,36	-	7.52	7.52	2.55	10.07
3598,12	0.39	6	6.39	2.17	8.56	3648,37	0.65	7.37	8.02	2.72	10.75
3599,23	0.61	4.87	5.48	1.86	7.34	3650,31	1.31	7.19	8.5	2.89	11.39
3601,26	0.63	4.6	5.23	1.78	7.01	3651,56	-	6.91	6.91	2.35	9.26
3603,28	0.55	5.27	5.82	2	7.80	3652,38	-	4.51	4.51	1.53	6.04
3605,26	0.58	5.28	5.86	2	7.85	3654,41	-	5.31	5.31	1.80	7.11
3605,86	0.34	3.62	3.96	1.35	5.30	3656,45	-	6	6	2.04	8.04
3607,35	0.58	5.02	5.6	1.90	7.50	3656,58	-	4.39	4.39	1.49	5.88
3609,38	0.64	4.57	5.21	1.77	6.98	3659,35	-	6.08	6.08	2.06	8.15
3610,11	0.34	3.35	3.69	1.25	4.95	3660,25	-	6.94	6.94	2.36	9.30
3611,23	0.88	4.93	5.81	1.98	7.79	3663,4	-	7.11	7.11	2.42	9.52
3613,26	0.62	4.91	5.53	1.88	7.41	3665,71	-	7.59	7.59	2.58	10.17
3613,53	0.44	5.3	5.74	1.95	7.69	3666,35	-	7.18	7.18	2.44	9.62
3614,39	0.63	5.03	5.66	1.92	7.58	3668,44	-	7.48	7.48	2.54	10.02
3617,48	0.9	5.06	5.96	2.02	7.99	3669,7	1.21	7.85	9.06	3.08	12.14
3617,67	1.2	7.42	8.62	2.93	11.55	3670,31		7.71	7.71	2.62	10.33
3619,38	1.3	4.82	6.12	2.08	8.20	3672,41		7.83	7.83	2.66	10.49
3621,36	0.52	5.1	5.62	1.91	7.53	3673,06		2.51	2.51	0.85	3.36

Table 12: Computations of the numerical application of the evaporitic loss and the S1 well correction Z-1

The variation profiles of the free potential S1 and the corrected free potential S1* for well depth Z-1 illustrate that the correction of S1 accounts for the actual amount of hydrocarbons in the source rock. Additionally, the mean S1 increases from 5.34 mg HC/g to 8.17 mg HC/g after correction (Fig 22).

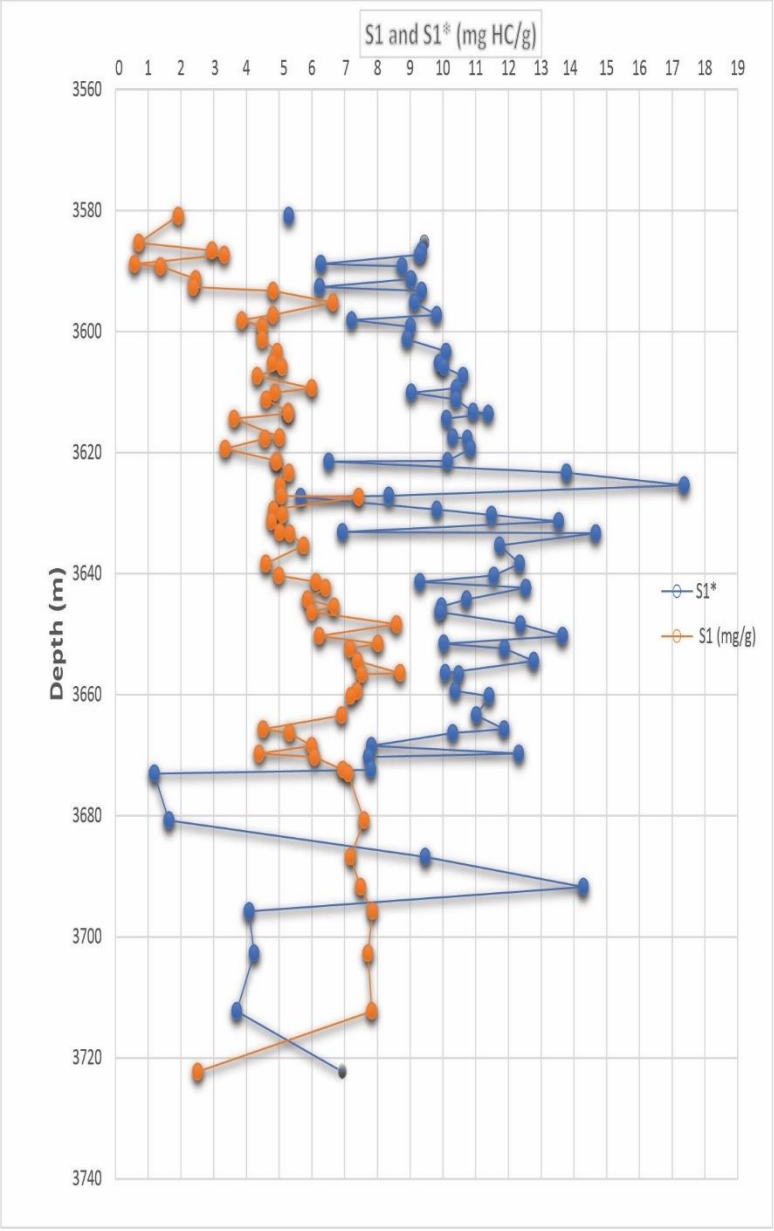

Figure 22: Variation profiles of free potential S1 and free potential S1* corrected for well depth Z-1.

4. Determination of Hydrocarbon Saturated Intervals

The geochemical phenomenon known as the oil crossover effect is observed during the evaluation of source rocks, representing a correlation between the total organic carbon content (TOC) and the fraction of generated hydrocarbons (S1). This parameter serves as a significant indicator of the oil potential of the source rock. The saturated intervals of hydrocarbons, as depicted in the profile (Fig. 23), are determined as a function of the depth of well Z-1.

The variation profiles of corrected free potential and the amount of TOC along the depth of well Z-1 demonstrate that the saturated intervals within the Frasnian bedrock vary with depth. This variation can be attributed to the coexistence of complex mineralogical components and non-clay minerals.

The mineralogical composition of a source rock can profoundly influence its capacity to generate, store, and release hydrocarbons. Certain minerals, notably clay, can affect the adsorption of hydrocarbons.

The Oil Saturation Index (OSI) provides insight into the saturated intervals of the Frasnian source rock and is calculated using the following formula

$$OSI = 100 * (S1^* / TOC)$$

Where:

- OSI: Oil Saturation Index
- S1*: Corrected Free Potential
- TOC: Total Organic Carbon

The OSI index helps gauge the oil saturation levels within the Frasnian source rock, contributing valuable information to the assessment of its hydrocarbon potential.

The obtained results are summarized in table 13

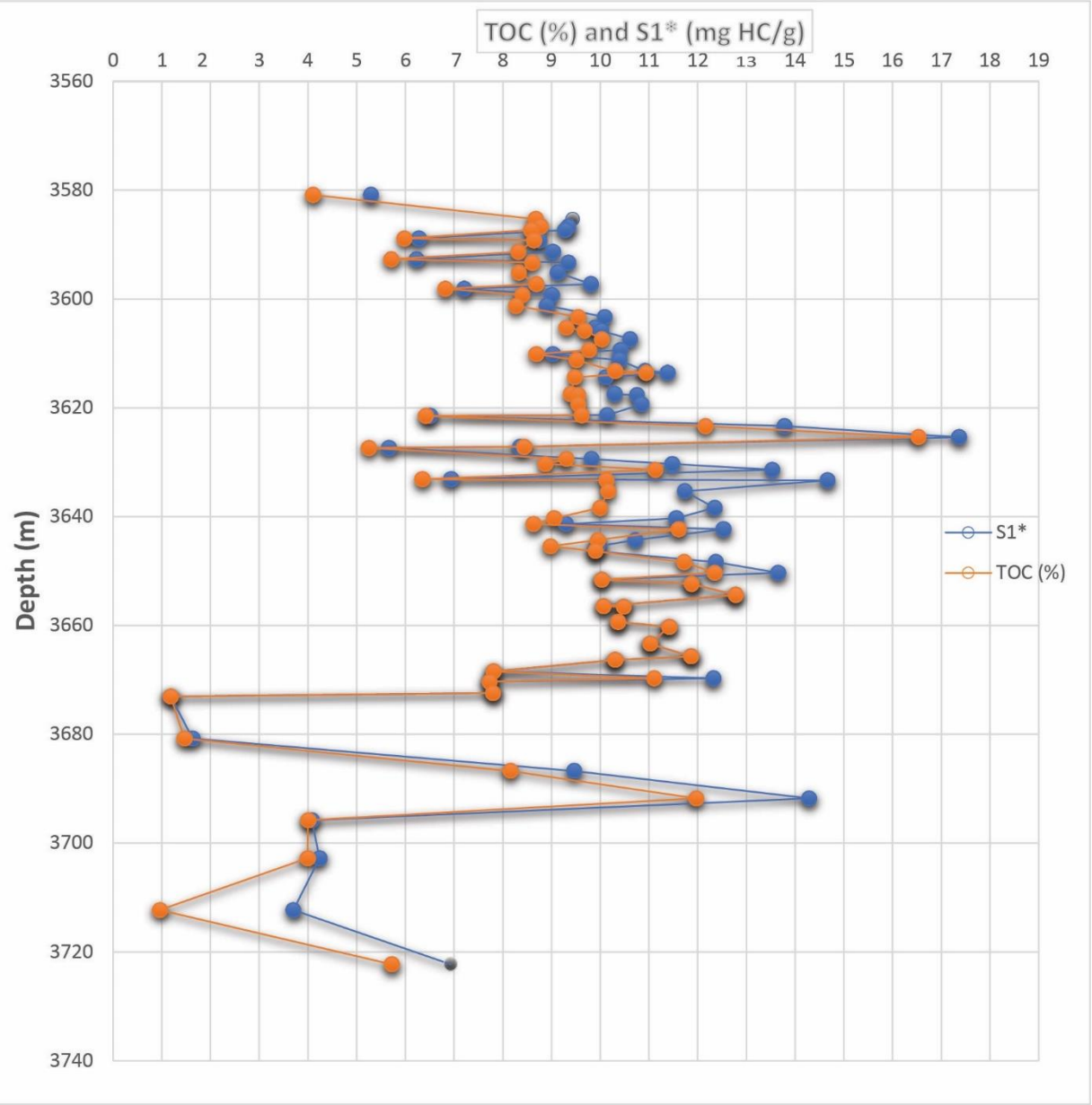

Figure 23: Free potential variation profiles corrected and TOC as a function of well depth Z-1.

Depth(m)	TOC (%)	S1* (mg/g)	OSI	Depth(m)	TOC (%)	S1* (mg/g)	OSI
3580,88	4,10	5,3	129,02	3621,47	6,42	6,5	101,40
3680,78	1,46	1,6	111,64	3623,36	12,15	13,8	113,33
3686,78	8,15	9,5	116,07	3625,41	16,53	17,4	105,02
3691,78	11,97	14,3	119,38	3627,14	8,44	8,4	98,93
3695,78	4,00	4,1	102,00	3627,38	5,25	5,7	107,81
3702,78	3,99	4,2	106,27	3629,41	9,29	9,8	105,60
3712,28	0,96	3,7	385,42	3630,31	8,87	11,5	129,43
3722,28	5,72	6,9	121,15	3631,38	11,14	13,5	121,55
3585,34	8,67	9,4	108,88	3633,12	6,35	6,9	109,13
3586,64	8,78	9,4	106,49	3633,34	10,13	14,7	144,83
3587,33	8,58	9,3	108,16	3635,34	10,16	11,7	115,45
3588,86	5,98	6,3	104,85	3638,36	10,00	12,3	123,51
3589,25	8,64	8,7	101,27	3640,34	9,05	11,6	127,62
3591,33	8,32	9,0	108,54	3641,36	8,63	9,3	107,65
3592,69	5,71	6,2	109,11	3642,31	11,61	12,5	107,93
3593,28	8,60	9,3	108,72	3644,3	9,95	10,7	107,74
3595,18	8,33	9,1	109,48	3645,43	8,98	10,0	110,80
3597,28	8,69	9,8	112,89	3646,36	9,90	9,9	100
3598,12	6,82	7,2	105,72	3648,37	11,72	12,4	105,55
3599,23	8,40	9,0	107,26	3650,31	12,34	13,7	110,61
3601,26	8,27	8,9	107,62	3651,56	10,03	10,0	100
3603,28	9,55	10,1	105,76	3652,38	11,88	11,9	100
3605,26	9,31	9,9	106,23	3654,41	12,77	12,8	100
3605,86	9,68	10,0	103,51	3656,45	10,07	10,1	100
3607,35	10,03	10,6	105,78	3656,58	10,48	10,5	100
3609,38	9,77	10,4	106,55	3659,35	10,36	10,4	100
3610,11	8,69	9,0	103,91	3660,25	11,41	11,4	100
3611,23	9,51	10,4	109,25	3663,4	11,02	11,0	100
3613,26	10,30	10,9	106,02	3665,71	11,87	11,9	100

3613,53	10,94	11,4	104,02	3666,35	10,30	10,3	100
3614,39	9,48	10,1	106,65	3668,44	7,81	7,8	100
3617,48	9,39	10,3	109,58	3669,7	11,11	12,3	110,89
3617,67	9,55	10,8	112,57	3670,31	7,72	7,7	100
3619,38	9,55	10,8	113,61	3672,41	7,80	7,8	100
3621,36	9,62	10,1	105,40	3673,06	1,18	1,2	100

Table 13: Calculations of the OSI (oil saturation index) well Z-1 index

The variation profile indicates that the depths ranging from 3700m to 3725m exhibit significant hydrocarbon saturation. Additionally, the OSI values exceeding 100 suggest a potentially substantial oil potential in these intervals. This observation underscores the likelihood of encountering viable oil reservoirs within this depth range (Fig. 24)

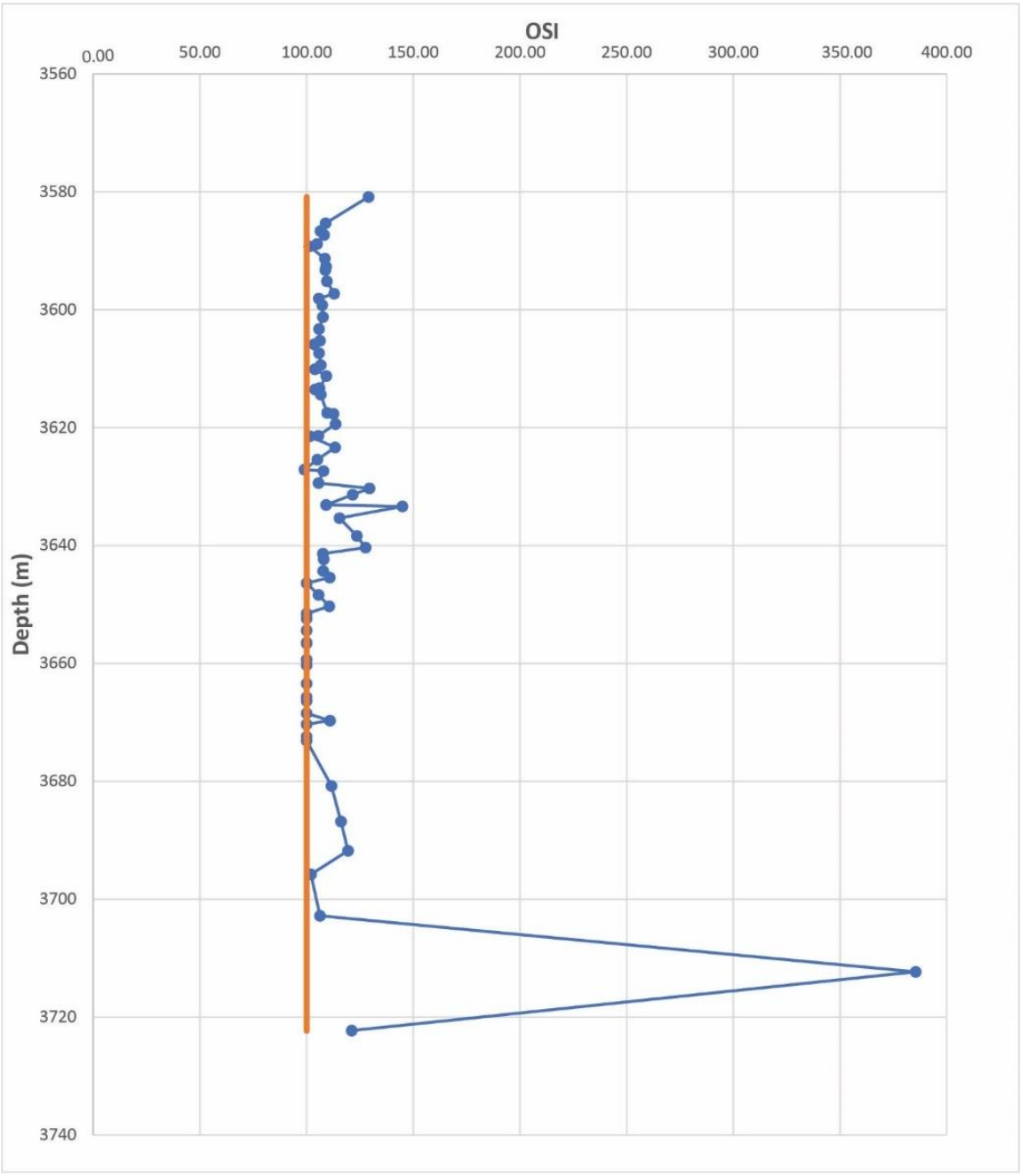

Figure 24: OSI oil saturation index variation profile as a function of Z-1 well depth.

5. Mass to volume conversion

In estimating the volume of hydrocarbons from source rocks, mass-to-volume conversion plays a pivotal role in deriving a volumetric estimation of the hydrocarbons within the rock.

Mass-to-volume conversion relies on crucial factors, including rock density and mass. For our specific scenario:

- Rock density: 2.5
- Hydrocarbon density: 0.7467 (API of 58)

The volume of hydrocarbons is determined using the formula:

$$Vol(m^3/m^3)=S1*\times 10-3\times\gamma Vol$$

Where:

- Vol: Volume in place
- S1*: Corrected Free Potential
- γ\gammaγ: Density ratio

In our case, γ\gamma equals 3.348 (L/m^3).

This calculation enables the conversion of mass-based parameters, such as the corrected free potential, into volume-based estimates, facilitating a comprehensive assessment of the hydrocarbon volume within the source rock.

The obtained results are summarized in table 14

Depth(m)	S1* (mg/g)	VOL (m^3/m^3)	Depth(m)	S1* (mg/g)	VOL (m^3/ m^3)
3580.88	4.1674	0.013952	3621.47	6.5124	0.021804
3680.78	1.1792	0.003948	3623.36	8.8976	0.029789
3686.78	5.7084	0.019112	3625.41	8.241	0.027591
3691.78	7.5576	0.025303	3627.14	7.5844	0.025393
3695.78	0.8844	0.002961	3627.38	6.7	0.022432
3702.78	2.1842	0.007313	3629.41	7.3834	0.02472
3712.28	6.9546	0.023284	3630.31	11.6982	0.039166
3722.28	4.8106	0.016106	3631.38	11.8054	0.039524
3585.34	7.4772	0.025034	3633.12	8.6162	0.028847
3586.64	9.6748	0.032391	3633.34	15.0348	0.050337
3587.33	7.3834	0.02472	3635.34	10.1304	0.033917
3588.86	5.561	0.018618	3638.36	14.6462	0.049035
3589.25	6.1506	0.020592	3640.34	11.6848	0.039121
3591.33	6.9546	0.023284	3641.36	11.6312	0.038941
3592.69	7.3164	0.024495	3642.31	10.8138	0.036205
3593.28	7.4236	0.024854	3644.3	10.9344	0.036608
3595.18	7.8658	0.026335	3645.43	12.9444	0.043338
3597.28	7.303	0.02445	3646.36	10.0768	0.033737
3598.12	8.5626	0.028668	3648.37	10.7468	0.03598
3599.23	7.3432	0.024585	3650.31	11.39	0.038134
3601.26	7.0082	0.023463	3651.56	9.2594	0.031
3603.28	7.7988	0.02611	3652.38	6.0434	0.020233
3605.26	7.8524	0.02629	3654.41	7.1154	0.023822
3605.86	5.3064	0.017766	3656.45	8.04	0.026918
3607.35	7.504	0.025123	3656.58	5.8826	0.019695
3609.38	6.9814	0.023374	3659.35	8.1472	0.027277
3610.11	4.9446	0.016555	3660.25	9.2996	0.031135
3611.23	7.7854	0.026066	3663.4	9.5274	0.031898
3613.26	7.4102	0.024809	3665.71	10.1706	0.034051
3613.53	7.6916	0.025751	3666.35	9.6212	0.032212
3614.39	7.5844	0.025393	3668.44	10.0232	0.033558
3617.48	7.9864	0.026738	3669.7	12.1404	0.040646
3617.67	11.5508	0.038672	3670.31	10.3314	0.03459

3619.38	8.2008	0.027456	3672.41	10.4922	0.035128
3621.36	7.5308	0.025213	3673.06	3.3634	0.011261

Table 14: Computations of the numerical application the mass to volume conversion of hydrocarbons from wells Z-1

The hydrocarbon volume variation profile with respect to well depth Z-1 indicates a notable presence of hydrocarbons within the Frasnian source rock. On average, the hydrocarbon volume in well Z-1 measures approximately 0.0241567 m^3/m^3 of rock. Notably, the interval spanning depths from 3630m to 3640m stands out due to its significantly higher volume compared to other levels within the well. This interval presents an intriguing prospect for potential hydrocarbon accumulation within the Frasnian reservoir.

(Fig. 25)

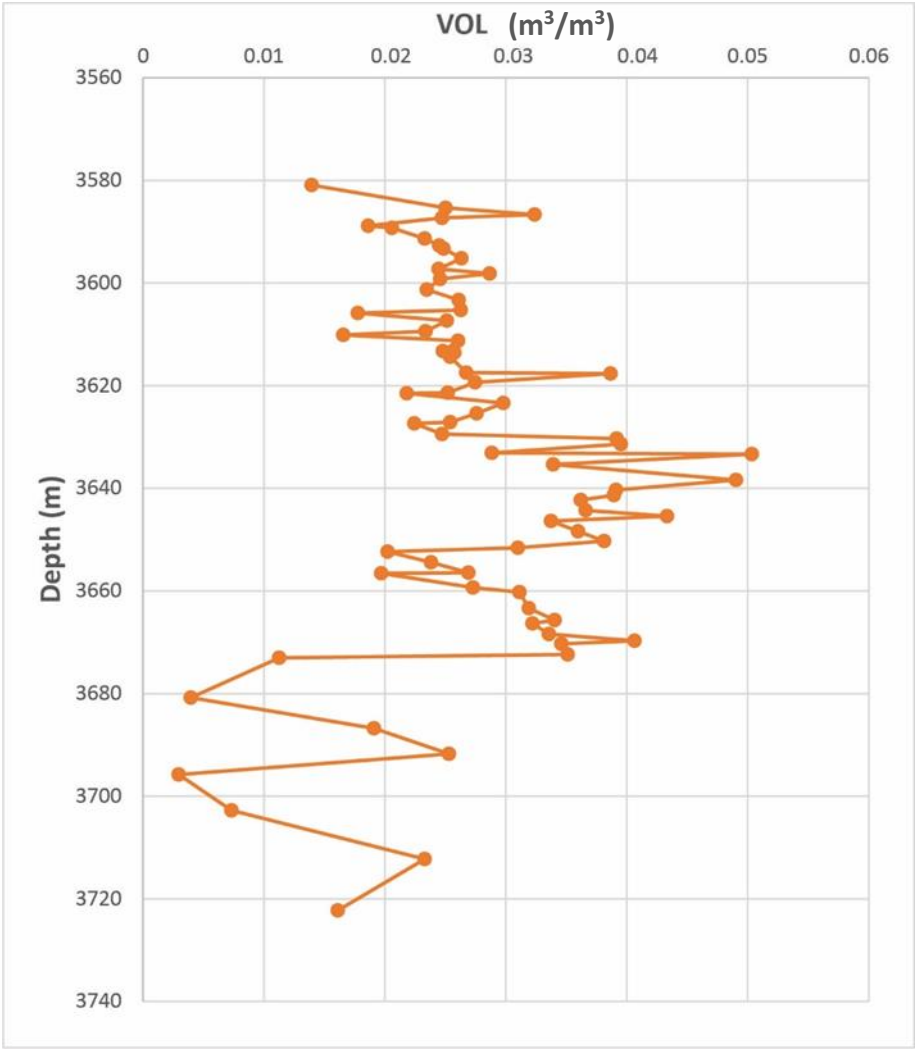

Figure 25: Hydrocarbon volume variation profile as a function of well depth Z-1.

6. Conclusion:

In summary, the analysis of the Frasnian source rock in well Z-1 provides valuable insights into its petroleum potential and guides further exploration endeavors:

- The profile of absorbed hydrocarbons across depths underscores significant quantities, notably observed between 3620m and 3640m, crucial for understanding the petroleum potential.
- Evaporitic loss estimation reveals a substantial loss of free hydrocarbons, prompting a correction to the free potential (S1*) to accurately assess the hydrocarbon content.
- Assessment of hydrocarbon-saturated passages, as indicated by the oil saturation index (OSI), identifies depths between 3700m and 3725m as promising zones with good hydrocarbon saturation, suggesting potential oil-rich reservoirs.
- Mass-to-volume conversion calculations demonstrate a relatively high volume of hydrocarbons within the Frasnian source rock, with an average volume of 0.0241567 m^3/m^3 of rock in well Z-1. Notably, the interval between depths of 3630m and 3640m stands out for its elevated hydrocarbon volume compared to other levels in the well. These findings collectively underscore the promising petroleum potential of the Frasnian source rock in well Z-1 and inform strategic exploration efforts.

CHAPTER 6:

"Integration of Artificial Intelligence in Estimating Hydrocarbon Potential: Enhancing Exploration Strategies"

1. Introduction to a Python Script Demonstrating Workflow for Predicting Geological Properties

The Python script provided below outlines a comprehensive workflow for handling geological data. It encompasses various stages including data preprocessing, feature selection, model training, prediction, and evaluation. Key Python libraries such as pandas, numpy, and scikit-learn are utilized throughout the script to facilitate data manipulation, scaling, regression, and model evaluation processes.

The primary goals of this script are to predict two crucial geological properties: Total Organic Carbon (TOC) percentage and Volume (VOL) based on the provided dataset. Additionally, the script aims to enhance model performance through feature selection techniques and assess the predictive capabilities of the models on new data

2. Methodology

The code executes the following tasks:

2.1.Data Loading and Preprocessing:

- Utilizes pandas to load data from a CSV file.
- Converts '-' entries to NaN values.
- Replaces missing values with 0.

```
import pandas as pd
import numpy as np
from sklearn.preprocessing import StandardScaler
from sklearn.linear_model import LinearRegression
from sklearn.metrics import mean_squared_error, r2_score
from sklearn.feature_selection import RFE
from sklearn.model_selection import train_test_split
```

Replaces missing values with 0 after converting '-' to NaN.

```
df = pd.read_csv("Train.csv")
df.replace('-', float('nan'), inplace=True)
df.fillna(0, inplace=True)
```

2.2.Feature Engineering and Target Separation:

Separates the dataset into features and target variables for predicting Total Organic Carbon (TOC) and Volume (VOL)

```
X = df.drop(columns=['TOC (%)', 'VOL (m3/m3)'])
y_toc = df['TOC (%)']
y_vol = df['VOL (m3/m3)']
```

2.3.Data Scaling:

Standardizes the features using StandardScaler from the scikit-learn library.

```
scaler = StandardScaler()
X_scaled = scaler.fit_transform(X)
```

2.4.Train-Test Split:

Splits the data into training and testing sets for both Total Organic Carbon (TOC) and Volume (VOL) predictions.

```
X_train_toc, X_test_toc, y_train_toc, y_test_toc = train_test_split(X_scaled, y_toc, test_split(X_scaled, y_toc, test_size=0.2, random_state=42)
X_train_vol, X_test_vol, y_train_vol, y_test_vol = train_test_split(X_scaled, y_vol, test_split(X_scaled, y_vol, test_size=0.2, random_state=42)
```

2.5.Feature Selection:

Initializing the Linear Regression Model

```
model = LinearRegression()
```

Utilizes Recursive Feature Elimination (RFE) to select important features for prediction.

-Selects 3 features for TOC prediction and 5 features for VOL prediction

```
selector_toc = RFE(model, n_features_to_select=3, step=1)
selector_toc.fit(X_train_toc, y_train_toc)
X_train_toc_selected = selector_toc.transform(X_train_toc)
X_test_toc_selected = selector_toc.transform(X_test_toc)
```

2.6.Model Training and Evaluation:

Trains separate Linear Regression models for TOC and VOL predictions.

```
model_toc = LinearRegression()
model_toc.fit(X_train_toc_selected, y_train_toc)
```

Evaluates model performance using Mean Squared Error (MSE) and R-squared metrics.

```
y_pred_vol = model_vol.predict(X_test_vol_selected)
mse_vol = mean_squared_error(y_test_vol, y_pred_vol)
r2_vol = r2_score(y_test_vol, y_pred_vol)
print(f'Volume Prediction with Feature Selection - Mean Squared Error: {mse_vol}, R-squared: {r2_vol}')
```

2.7.Prediction on New Data:

- Loads new data from a CSV file.

- Scales and selects features for TOC and VOL predictions using the trained models.

- Predicts TOC and VOL values for the new data.

```
new_data = pd.read_csv("Predict.csv")
new_data_scaled = scaler.transform(new_data)
new_data_selected_toc = selector_toc.transform(new_data_scaled)
new_data_selected_vol = selector_vol.transform(new_data_scaled)
new_toc_predictions = model_toc.predict(new_data_selected_toc)
new_vol_predictions = model_vol.predict(new_data_selected_vol)
print("Predicted TOC values for new data: ", new_toc_predictions)
print("Predicted Volume values for new data: ", new_vol_predictions)
```

2.8.Evaluation Metrics on New Data:

-Compares the predicted TOC and VOL values with the actual values from the new data.

-Calculates MSE and R-squared metrics to evaluate the model's performance on the new data.

```
actual_toc = np.array([...])  # The actual TOC values for the new data
mse_toc = mean_squared_error(actual_toc, new_toc_predictions)
r2_toc = r2_score(actual_toc, new_toc_predictions)
print("TOC Prediction Metrics on New Data:")
print(f"Mean Squared Error (MSE): {mse_toc}")
print(f"R-squared: {r2_toc}")

actual_vol = np.array([...])  # The actual VOL values for the new data
mse_vol = mean_squared_error(actual_vol, new_vol_predictions)
r2_vol = r2_score(actual_vol, new_vol_predictions)
print("Volume Prediction Metrics on New Data:")
print(f"Mean Squared Error (MSE): {mse_vol}")
print(f"R-squared: {r2_vol}")
```

2.9.The new set of data (TOC and VOL) :

```
actual_toc = np.array([5.33, 2.95, 6.85, 7.37, 9.43, 8.43, 7.24, 8.81, 7.24, 5.24, 7.04, 6.3, 7.03, 4.76, 7.85,
                       5.97,7.96, 9.42, 4.09, 7.45, 4.9, 8.97, 11.74, 5.15, 9.28, 8, 8.36, 5.86, 6.01, 8.87,
                       12, 10.95, 5.49, 4.92, 6.21, 7.84, 10.27, 11.25, 9.59, 11.75, 8.35, 7.5, 5.69, 8.29, 8.57, 9.45,
                       11.43, 7.45, 10.76, 6.7, 7.46, 7.99, 11.55, 4.54, 11.21, 6.96, 10.03, 7.93, 7.78, 8.96, 11.12,
                       10.61, 7.19, 6.55, 8.14, 8.28, 8.39, 7.08, 1.9, 4.26, 8.9, 7.72, 2, 6.9, 3.88, 4.09, 6.51, 1.17,
                       10.73, 4.12])
mse_toc = mean_squared_error(actual_toc, new_toc_predictions)
r2_toc = r2_score(actual_toc, new_toc_predictions)

print("TOC Prediction Metrics on New Data:")
print(f"Mean Squared Error (MSE): {mse_toc}")
print(f"R-squared: {r2_toc}")

actual_vol = np.array([0.013937032, 0.015738778, 0.027503117, 0.020084165, 0.0290399, 0.024641521, 0.02734414,
                       0.024535536, 0.025595387, 0.01494389, 0.024164589, 0.021091022, 0.00736596, 0.029728803,
                       0.009273691, 0.03661783, 0.026231297, 0.00842581, 0.033173317, 0.008584788, 0.033703242,
                       0.025966334, 0.028721945, 0.005829177, 0.014413965, 0.033279302, 0.032007481, 0.033491272,
                       0.005140274, 0.017699501, 0.020296135, 0.02103803, 0.027821072, 0.042658978, 0.030629676,
                       0.026973192, 0.03534601, 0.004769327, 0.042341022, 0.024800499, 0.005617207, 0.024588529,
```

We observe the following:

-The average of volume values is approximately 0.023730218 m^3/m^3

- The average of TOC values is approximately 7.4893 %

3. Accuracy Discussion:

The graphs (Fig 26-Fig 27) compare the actual and predicted values of TOC (Total Organic Carbon Fig. 26) and volume (Fig.27) for new data. In both graphs, the X-axis represents actual values, the Y-axis represents predicted values, and the diagonal line indicates perfect predictions. The R^2 value of 0.52 means that the model explains 52% of the variance in the actual values, indicating a moderate accuracy of the model's predictions for TOC and volume.

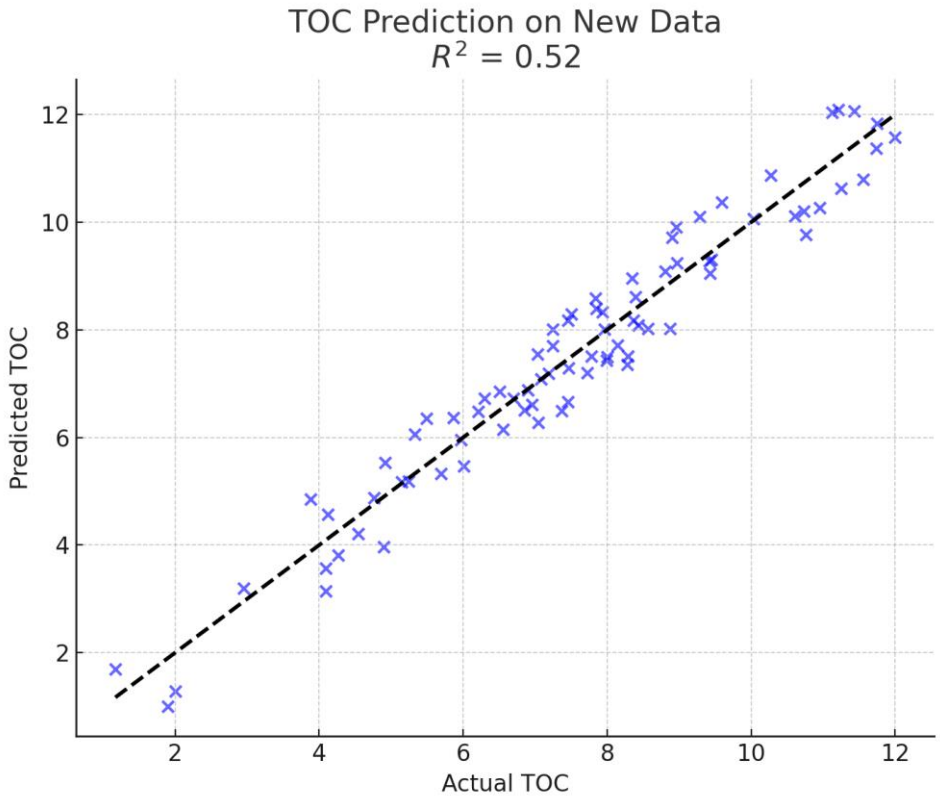

Figure 26: TOC Prediction on New Data

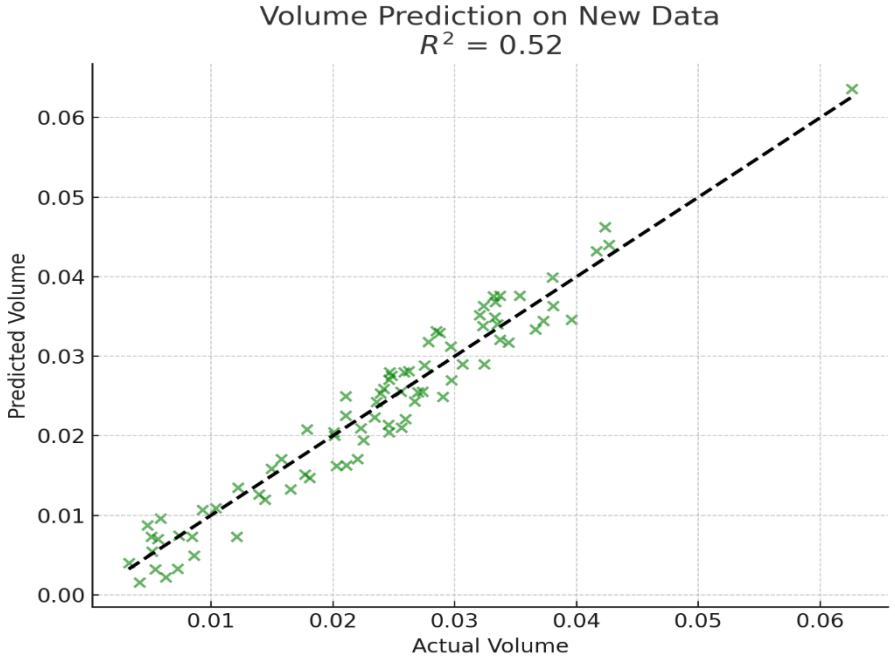

Figure 27: Volume Prediction on New Data

4. Conclusion:

The analysis demonstrates promising results, with an average volume of approximately 0.023730218 m^3/m^3 and an average TOC value of around 7.4893%. Furthermore, the positive R-squared value of 0.523849587 indicates that the predictive models effectively match the variance of Total Organic Carbon (TOC) and Volume (VOL) based on geological data. This alignment suggests that approximately 52.38% of the variability in TOC and VOL is accurately captured by the models, emphasizing their effectiveness in geological analysis and prediction tasks.

General conclusion:

The comprehensive analyses conducted on the Frasnian deposits in well **Z-1** provide valuable insights into sedimentology, petrography, mineralogy, and petroleum potential assessments. Here are the key findings synthesized from these analyses:

- Sedimentological, petrographic, and mineralogical investigations characterize the Frasnian deposits in well Z-1 as part of a distal marine platform environment characterized by anoxic, low-energy conditions.
- Five distinct lithofacies associations are identified, each exhibiting unique mineral compositions, validated through petrographic and SEM analyses.
- Diagenetic processes, including carbonate cementation, silicification, recrystallization of bioclasts, and pyrite cementation, have influenced reservoir qualities.
- Petroleum potential assessments reveal:

    - Average Total Organic Carbon (TOC) content of 8.88%, classified as excellent.
    - Average free potential (S1) of 5.34 mg HC/g, rated as excellent.
    - Average residual potential (S2) of 4.90 mg HC/g, classified as good.
    - Thermal maturation analysis indicating advanced maturity and wet gas generation.
    - Microscopic analysis suggesting high initial potential, classified as type II organic matter.
    - The Thermal Alteration Index (TAI) indicating a transition between wet and dry gas generation.

- Hydrocarbon assessments unveil:

    - Notable abundance of absorbed hydrocarbons, particularly between depths of 3620m and 3640m.
    - Substantial evaporitic loss, with necessary corrections applied.
    - Identification of potential oil-rich zones, especially between depths of 3700m and 3725m.

    - Relatively high volume of hydrocarbons, notably between depths of 3630m and 3640m.

- Predictive models exhibit moderate success, capturing approximately 52.38% of the variability in TOC and volume based on geological data.

These findings collectively underscore the promising petroleum potential of the Frasnian source rock in well Z-1, providing valuable insights for further exploration and geological analysis.

References

Espitalie, J., Deroo, G., & Marquis, F. (1985). Rock-Eval Pyrolysis and its Applications. Review of the French Petroleum Institute.

Espitalie, J., Madec, M., Tissot, B., Mennig, J. J., & Leplat, P. (1977). Source rock characterization method for petroleum exploration. Proceedings of the Ninth Offshore Technology Conference, Houston, 439-442.

Heath, J. E., Dewers, T. A., Chidsey, T. C. Jr., Carney, S. M., & Bereskin, S. R. (2017). The gothic shale of the Pennsylvanian paradox formation, greater Aneth field (Aneth unit), southeastern Utah: Seal for hydrocarbons and carbon dioxide.

Jaeger, H., & Lampart, V. (2009). Palynology of the Upper to Middle Devonian of wells from the Reggane Basin, Southern Algeria.

Jaeger, H. (2019). A new workflow in unconventional shale play analysis.

Jarvie, D. M. (2008). Geochemical Characteristics of the Devonian Woodford Shale.

Jarvie, D. M. (2010). Worldwide Shale Gas and Oil Plays and Potential.

KASED Mohamed. (2013). The Shale Gas Potential in Algeria. SONATRACH.

Lafargue, E., Marquis, F., & Pillot, D. (1998). Rock Eval 6 applications in hydrocarbon exploration, production and oil contaminations studies. Revue Institut Français du Pétrole.

McKenna, J., & Hedley, R. (2002). The Structural Evolution of the Berkine-Ghadames Basin (Groupement Berkine Anadarko). Internal report, Anadarko Petroleum Corporation.

Michael, E. G., et al. (2014). Determination of In-Situ Hydrocarbon Volumes in Shale Plays.

Peters, K. E., & Cassa, M. R. (1994). Applied source rock geochemistry. AAPG Memoir 60.

Romero-Sarmiento, M.-F., et al. (2014). New Rock-Eval method for characterization of shale plays.

Schieber, J., & Zimmerle, W. Petrography of Shales: A Survey of Techniques. Department of Geology, The University of Texas at Arlington, Texas 76019, USA; Prinzengarten 6, D-29223 Celle, Germany.

SERBAH, S., Mokri, Y., & Guelil, K. (2019, February). Attempt of Sedimentological, Petrographic, Mineralogical, and Geochemical Characterization of the Frasnian Black Shales (Berkine Basin). Sonatrach DLAB Report.

Welton, J. E. (1984). SEM Petrology Atlas. The American Association of Petroleum Geologists, Tulsa, Oklahoma, USA.